

---

# VALUE PREDICTION FOR SPATIOTEMPORAL GAIT DATA USING DEEP LEARNING

---

A PREPRINT

Ryan Cavanagh<sup>1</sup>, Jelena Trajkovic<sup>1,\*</sup>, Wenlu Zhang<sup>1</sup>, I-Hung Khoo<sup>2</sup>, and Vennila Krishnan<sup>3</sup>

<sup>1</sup>*Department of Computer Engineering and Computer Science, California State University Long Beach*

<sup>2</sup>*Electrical Engineering and Biomedical Engineering, California State University Long Beach*

<sup>3</sup>*Department of Physical Therapy, California State University Long Beach*

*\*Corresponding author: Jelena.Trajkovic@csulb.edu*

March 14, 2024

## ABSTRACT

Human gait has been commonly used for the diagnosis and evaluation of medical conditions and for monitoring the progress during treatment and rehabilitation. The use of wearable sensors that capture pressure or motion has yielded techniques that analyze the gait data to aid recovery, identify activity performed, or identify individuals. Deep learning, usually employing classification, has been successfully utilized in a variety of applications such as computer vision, biomedical imaging analysis, and natural language processing. We expand the application of deep learning to value prediction of time-series of spatiotemporal gait data. Moreover, we explore several deep learning architectures (Recurrent Neural Networks (RNN) and RNN combined with Convolutional Neural Networks (CNN)) to make short- and long-distance predictions using two different experimental setups. Our results show that short-distance prediction has an RMSE as low as 0.060675, and long-distance prediction RMSE as low as 0.106365. Additionally, the results show that the proposed deep learning models are capable of predicting the entire trial when trained and validated using the trials from the same participant. The proposed, customized models, used with value prediction open possibilities for additional applications, such as fall prediction, in-home progress monitoring, aiding of exoskeleton movement, and authentication.

**Keywords** Gait Value Prediction; Recurrent Neural Network; Convolutional Neural Network; Time-series Gait Data; Health Monitoring; Rehabilitation; Wearable Technology

## 1 Introduction

Clinical gait analysis has been used in the diagnostic, assessment, monitoring, and prediction of health conditions Baker et al. [2016]. For example, human gait can be used as an important diagnostic indicator to discern pathological conditions such as stroke, Parkinson's disorders, and other neuro-musculoskeletal conditions, from normal. Traditionally, to establish a diagnosis of the gait disorder, a trained clinician would either analyze a participant using observational gait analysis, quantitatively record (pathological) gait via a motion capture system, or record spatiotemporal gait parameters. While trained clinicians provide needed expertise, their observation, and analysis are subjective and they are usually not available outside of the clinical environment or for an extended time (e.g. for in-home rehabilitation or monitoring). Therefore, quantitative gait measurement and analysis are valuable aids in diagnosis as well as in the prognosis of a disorder as they can facilitate objective monitoring and data acquisition for long time periods.

Recent innovations in technology allow quantitative gait data acquisition, that removes subjectivity and the need for prolonged clinical observation by an expert. Apart from the gold-standard motion capture system, which is expensive and labor-intensive Mob, a variety of sensor-based systems have been used to monitor or analyze gait. For example, devices that sense pressure and motion are attached to feet (Walk-Even insole I.-H. et al. [2015], SmartShoe Bae

et al. [2009], Kong et al. [2008]) or knees, thighs, and hips Mannini and Sabatini [2011] to record the spatiotemporal parameters of gait. Innovation in technology also expands applications beyond clinical use. For example, gait analysis has been used for biometric identification Potluri et al. [2019], Moon et al. [2020a], for detecting impaired driving Li et al. [2019], sports activity Ghazali et al. [2018], or (general) human activity Lee et al. [2019a]. Hence, contemporary sensor-based monitoring and data acquisition systems facilitate a more objective, quantitative assessment of gait, while being portable, accurate, easily available, and less expensive.

The above advances in gait data acquisition have enabled new applications based on statistical and machine-learning models (see Section 2). However, there still remains a large gap in gait modeling and analysis that is tuned to the individual under observation, is easy to extend to new individuals, and can be used in real-time applications. We address this gap by proposing a technique to generate *accurate* and *customized* deep-learning models to predict spatiotemporal gait data for *each* individual. Our models can be used to aid professionals in rehabilitation or prognosis, in clinical and in-home environments. Target applications include qualitative and quantitative feedback to post-stroke survivors Lee et al. [2019b], aiding exoskeleton motion Aertbeliën and Schutter [2014] or fall prediction Schniepp et al. [2021]. Moreover, as our models are customized to a particular individual, they can be used for authentication by providing a *quantitative metric* of (dis)similarity of spatiotemporal gait parameters helping us identify a participant as one of known (in the dataset) or unknown individuals (not in the dataset).

The specific contributions of this work are:

- C.1 We generate a set of deep-learning model architectures for short-distance and long-distance *value prediction* for sensor data corresponding to human gait. While other works use gait-related data for classification, we can successfully predict actual values. Our models that target long-distance prediction can predict the *entire trial*. Not only the proposed models *expand beyond classifiers*, but they are also suitable to provide quantitative data for use in patient recovery, fall risk assessment, fall prediction, and in aiding exoskeleton movement.
- C.2 We propose architectures that can train *individually* on the data from either each trial or from multiple trials from each participant, thus generating the models with the following advantages:
  - C.2.a Unlike traditional deep-learning models, which are trained on data with a large number of features, all our models are trained on data with a smaller number of features. Despite this challenge, the proposed approach yields *customized models* that have been shown to have *high accuracy*.
  - C.2.b We show that our models can predict the values in a *fraction of the time* needed for a participant to make a move and generate new data. Therefore, the proposed models can be used in *real-time applications* that require high accuracy, such as patient monitoring.
  - C.2.c In contrast to the majority of other applications, there is *no need to re-train one large unified model* using all training data when a new participant is added to the study. We only need to train a single new model for the new participant, thus saving on training time.
- C.3 We *expand the application* of deep learning models (ensemble CNN+RNN models) to predict *time-series spatiotemporal gait data values*. This is an application beyond typical use for the analysis of image caption data, and financial data.

## 1.1 Overview of the Proposed Method

We utilize a dataset obtained from Walk-Even insoles I.-H. et al. [2015], where each shoe insole is equipped with six sensors. Therefore, each trial records six sensor values from each foot as the participant applies pressure while walking at a regular pace. We predict the consecutive pressure values that correspond to each of the six sensors on the right foot.

We propose a technique to train four deep learning model architectures for each individual to predict the pressure values of gait cycles: RNN with a single RNN layer, LSTM (Long Short Term Memory) with two LSTM layers, Bidirectional LSTM with two bidirectional LSTM layers, and an ensemble CNN+RNN combining two 1-Dimensional convolutional layers and an LSTM layer. The first three models are designed to predict short sequential data, while the CNN+RNN model is designed to predict long sequential data. Usually, CNN+RNN architectures are designed to deal with image captioning analysis but in this project, we leverage CNN+RNN architecture to preserve temporal features in long-distance gait data. Specifically, CNN is used to shorten the input data while maintaining the overall patterns. Working with temporal data sets, combining CNN and RNN has been shown to improve prediction outcomes while lowering computational costs compared to traditional RNN models.

We present two experimental setups, ‘by trial’ and ‘by participant’. Setup ‘by trial’ is applied to a single gait trial to explore the ability of different models to make a short-distance prediction. Setup ‘by participant’, is applied to multiple concatenated trials, from a single participant, to explore the ability of different CNN+RNN models to make a long-distance prediction, i.e. the ability to predict entire trials. We evaluate model accuracy using standard evaluation

metrics, MAE (Mean Absolute Error), MSE (Mean Squared Error), and RMSE (Root Mean Squared Error), to calculate how closely the predicted time series data matches the actual time series (sensor) data. Both setups train on data obtained from the six sensors for the right foot that, in turn, predict the values for the same sensors in the next time steps. MAE, MSE, and RMSE values are computed using predicted values for each sensor. To provide a visual comparison and showcase the quality of prediction, the sensor data for individual sensors (i.e. true test data values) are summed up at each time step and plotted alongside the sum of predicted data for the corresponding time step. Our results show that the best-performing model for a short sequence prediction is Bidirectional LSTM with an average RMSE = 0.124346 and a minimum RMSE = 0.060675. The best-performing model for long-distance prediction in the vast majority of cases is CNN+RNN with an average RMSE = 0.194171, and as low as RMSE = 0.106365. In a few cases, for an output window of 3 or 4 Bidirectional LSTM slightly outperforms CNN+RNN, but at the expense of increased complexity and run-time. Moreover, the proposed models for long-distance prediction can accurately predict an entire trial for a participant, when trained and validated using the trials from the same participant.

The rest of this paper is structured as follows: Section 2 reviews the previous works, and Section 3 provides the description of the dataset. Section 4 describes proposed modeling, and Section 5 presents the experimental results. We follow up with a discussion of limitations and future work (Section 6), and conclude in Section 7.

## 2 Related Work

Gait is the result of a cyclic series of movements and is characterized by the fundamental unit ‘gait cycle’. A gait cycle is defined as the sequence of events starting when a foot contacts the ground to when that same foot contacts the ground again. Typically, during human locomotion, the right foot is taken as the reference limb. A full gait cycle could be divided into two major phases: stance and swing. The stance phase occurs as the reference foot is on the ground, supporting the body’s weight. The swing phase occurs as the foot is in the air, being advanced for the next contact with the ground. At normal walking speed by a healthy participant, the stance phase occupies approximately 60% of the gait cycle, and the swing phase occupies the remaining 40%.

There have been numerous studies on gait, gait cycle analysis and classification, the applications of sensors (pressure, Inertial Measurement Unit (IMU), or other wearable sensors), and motion capture systems, to gait. We present the below studies that relate to the proposed work and point to possible future directions.

### 2.1 Gait Cycle Analysis, Deterministic and Statistical Modeling

The initial efforts that utilized sensor data for gait analysis used deterministic and statistical methods to analyze or classify the gait cycle or its phases. For example, Tong et al. Tong and Granat [1999] analyzed data from a gyroscope attached to the ankle to distinguish between straight and curved walking using correlation coefficients. Sabatini et al. Sabatini et al. [2005] analyzed angular change reported by an IMU sensor, to distinguish between gait cycle phases.

Moreover, the knowledge obtained from sensors collecting gait information can be applied to evaluate a person’s gait Rachel M Koldenhoven [2018], A. et al. [2018], Khoo et al. [2017]. Koldenhoven et al. Rachel M Koldenhoven [2018] conducted a validation study to compare gait cycle data obtained using wearable sensors (triaxial accelerometer and gyroscope) and the 3D motion capture system. They showed that the runner’s data could accurately be captured using wearable sensors outside traditional laboratory settings. Murai et al. A. et al. [2018] use IMU and a large-scale system (the commercial marker-based optical motion capture system with 15 cameras) to build a software model, using correlation coefficients. The model is then used with IMUs only, outside the lab, to assess risks for runner’s injury. Both systems show that wearable devices, with appropriate software, can provide reliable metrics for human locomotion.

Khoo et al. Khoo et al. [2017] also used gait cycle data to re-train post-stroke individuals using in-sole pressure sensors with real-time biofeedback. They measured the weight distribution of an individual’s foot and determined the asymmetry of gait. They used a deterministic algorithm for the gait phase analysis. We utilize the same data obtained by Khoo et al. [2017] but instead of deterministic algorithms for re-training we use deep learning modeling for value prediction for human gait.

Bae et al. Bae and Tomizuka [2011] utilized data collected from embedded air-bladder force sensors in a shoe insole to analyze the gait phases of healthy individuals. Their method builds a Hidden Markov Model (HMM) using the sensor-obtained values to detect gait phases and check for abnormal state transitions between the phases. Mannini et al. Mannini and Sabatini [2011] developed an HMM applicable to data collected from a foot-mounted gyroscope. The model detects the gait phases for individuals walking at different speeds and inclinations on the walking surface. Such systems enable accurate and automatic detection of gait cycles, which are essential for thorough gait analysis in normal as well as pathological populations. Our study differs concerning the objective of making predictions and the prediction

method used. Both aforementioned studies use a statistical model, HMM, for gait phase detection, while the proposed method uses deep learning on time series of gait data values for value prediction.

## 2.2 Machine Learning-Based Gait Analysis and Detection Algorithms

The use of sensors to better understand human gait has been merged with machine learning Costilla-Reyes et al. [2020], Wang et al. [2019], Potluri et al. [2019], Moon et al. [2020a]. Costilla-Rayes et al. Costilla-Reyes et al. [2020] present applications of deep learning in security and healthcare. Wang et al. Wang et al. [2019] survey the recent advance of deep learning-based sensor-based activity recognition. Parkka et al. Parkka et al. [2006] obtained data from various sensors (e.g. gyroscope, accelerometers, and physiological sensors) attached to eight body parts with the participants at different settings (e.g. walking or climbing stairs). They formulated machine learning models (decision tree and neural network) to classify one of seven activities that a participant is performing. Lee et al. Lee et al. [2019a] used the data from pressure and IMU sensor readings obtained from FootLogger insole Foo to construct a separate Convolutional Neural Network model for each type of input (sensor) to perform classification. The dataset in both studies has a significantly larger number of features than in our study. A large number of features usually makes for easier training of accurate machine and deep learning models. We design the models for using fewer features that can achieve high prediction accuracy. Unlike previous work which focuses on classification, we predict actual values in time-series data, setting us apart.

Moon et al. Moon et al. [2020b] showed that gait information can be used to distinguish between different individuals. FootLogger insoles Foo were used to record data from pressure and IMU sensors as the participants walked. They proposed a deep learning architecture that combined convolutional (CNN) and recurrent neural networks (RNN) to identify any of the tested participants. While the general idea of CNN+RNN architecture is similar to ours, the applications greatly differ. Moon et al. Moon et al. [2020b] aim to identify a person based on their previous gait data, while we can predict an entire trial based on previous gait data. Similarly to the previous studies, we work with much-reduced input data size, making the prediction modeling additionally challenging, yet successful.

Some studies found that customized (subject-specific) models have higher accuracy of prediction than unified (generic) models. Zhang et al. Zhang et al. [2020] discovered that subject-specific models outperformed the generic ones even though they did not need additional subject-specific characteristics. Similar findings have been reported for CNN models for a freeze of gait (FoG) detection Xia et al. [2018]. The intuition behind those results is that gait spatiotemporal data are unique for each individual (please see Figures 2 and 5), and furthermore, the data patterns might be different for the same individual between different/repeated trials (please see Figures 5 and 7). This motivated us to propose a technique that generates customized models. Furthermore, having customized models removes the need to retrain the global model. Retraining requires the use of the entire training data set, as in Chen and Xue [2015], Moon et al. [2020b] which consumes both processing time and memory, and it is likely not suitable for real-time applications. Contrary, the proposed, customized models would need to train only a single trial (for 'by trial' setup) or on all available trials for the newly added participant (for 'by participant' setup). Finally, the run time of model generation (training) and prediction (testing) are more efficient with the proposed approach due to the use of customized models.

Horst et al. Horst et al. [2019] devised a general framework that facilitates the understanding and interpretation of non-linear machine learning methods in gait analysis. They feed portions of the model's predictions back to the input variables to distinguish the variables that are most relevant for the characterization of gait patterns from a certain individual. The applications of sensor data analysis are not only limited to gait analysis but can also be applied to other areas of the body. Rawashdeh et al. Rawashdeh et al. [2016] used an IMU sensor attached to the upper arm of a person to track the motion of their shoulder to help prevent overuse injuries. They were able to classify the different positions of the shoulder and assess if repeated usage of the same form can cause injuries soon. Although not used in our methods, the characterization of inputs that are most influential to the output and the use of sensors positioned at different body parts are suitable directions for extensions of our work.

## 2.3 Value Prediction for Human Motion using Machine Learning and Deep Learning

Rudenko et al. Rudenko et al. [2020] surveyed and proposed a taxonomy for human motion trajectory prediction. While human motion can have many notions, such as "full-body motion, gestures/facial expressions, moving through space by walking, using a mobility device or driving a vehicle," only "moving through space by walking" may relate to our study, as it includes a prediction of the values of human motion, such as trajectory coordinates or velocity profile. Human motion trajectory prediction has started to utilize Machine Learning and Deep Learning for value prediction. For example, Saleh et al. Saleh et al. [2018] used LSTM architecture to predict the trajectories of pedestrians. The prediction models were trained and tested on (sequential) images from the moving vehicle's stereo cameras. Djuric et al. Djuric et al. [2018] proposed a CNN-based uncertainty-aware vehicle motion prediction approach that utilizes

high-definition map images containing the projected prior motion of the vehicle and surroundings. The model was capable of producing a short-distance trajectory of the vehicle alongside uncertainty. Finally, ensemble models that combine CNN and RNN (namely LSTM) have been used in this domain to combine "the spatial and temporal relations of the observed agent's motion" Rudenko et al. [2020]. Xue et al. [2018] introduced a hierarchical model where CNN was used to extract relevant information from the person's trajectory, social neighborhood, and global scene layout, and provide it to the LSTM model. Zhao et al. [2019] apply similar architecture on fused images of the environment and agents (both pedestrians and vehicles), thus capturing the interactions between the agents and forming a prediction. While previous deep learning architectures are similar to the proposed one, the nature of the input data, thus the application of those architectures, is very different. The motion trajectory prediction mainly uses sequences of images, thus having much more input (training) data and features. We carefully designed our models, through experimentation, to have high accuracy despite the small number of features.

Ogata and Matsumoto [2019] proposed a method to estimate the joint angles of the upper human body. They collected data using a wearable suit implanted with strain sensors. They utilized a CNN model to estimate the joint angle values for bending and straightening an elbow. Utilization of similar sensing mechanisms, and corresponding prediction modeling, is a promising direction for our future work, namely the application of value prediction for aiding exoskeleton movement.

## 2.4 Dataset Size

The number of participants also referred to as a sample size, their age, and health status are challenges for many machine learning and deep learning studies related to gait. Recent surveys Harris et al. [2022], Saboor et al. [2020], Ren and Peng [2019] illustrate the challenge. Harris et al. [2022] point out that a sample size is a concern across surveyed work: "With the clinical nature of these studies and the impaired gait participants they require, the barriers to experimentally collecting sufficient data are understandable". As per Lingmei et al. [2019], the issue is even more pronounced for fall detection and prevention since falls are very rare events. Harris et al., also, cite potential solutions to obtaining data that represents a larger number of participants and a wider range of health conditions. From the usage of medications to induce fatigued gait in healthy subjects Lasselin et al. [2020], to the use of generated, synthetic data Arifoglu and Bouchachia [2017] that reflect features similar to abnormal. Finally, the recent trend is to take data acquisition out of the lab Russell et al. [2021]. Cheng et al. [2017] used passive monitoring, using a smartphone over 24 weeks, which is very time-consuming both for data acquisition and processing. Additionally, the proposed workaround strategies, such as "aggregating, pre-processing, and learning the data", address cost, time, user privacy, and clinical constraints, hence, the resulting systems may be somewhat simple and introduce errors Harris et al. [2022].

Saboor et al. [2020] recognize the issue and illustrate its magnitude. Out of 33 surveyed papers from 2015 to 2020, 59% have a sample size of fewer than 30 participants (34% have 1 - 10, and 25% have 11 - 30). Only about 30% have more than 100 participants, and roughly a third of those collect the data using a device that is placed in the pocket or attached to a hand, indicating the use of an IMU sensor or a smartphone. While the use of an IMU sensor or a smartphone allows for a larger number of participants, longer monitoring, and ease of setup outside of the clinical environment, the accuracy of this approach has been reported as a challenge. Therefore, we propose to extend our approach to the use of IMU sensors and strain sensors in addition to the pressure sensors to expand applications but strive for accuracy. Complementary to the issue of dataset size is the issue of how the data is acquired while using sensor-based systems. The data acquisition and therefore accuracy of models derived from the data will depend on sensor location and their installation on the body McGinnis et al. [2017], Zhao and Zhou [2017], hence we will research sensor type and location needed for the proposed systems to be accurate.

## 3 Dataset

The data has been gathered in a controlled laboratory environment using a custom-made wearable device, called Walk-Even Khoo et al. [2017]. Walk-Even insoles are equipped with Force Resistive Sensors (FSR) placed on the front and back of the foot. Each insole has a total of six FSR pressure sensors: three on the heel ('back insole') and three on the front part of the foot ('front insole'). The three sensors are placed on top/bottom of each insole, but to the center and each side (toward the outer or inner edge of the foot). Walk-Even stores the raw data, produced by each sensor, in a control unit, worn on the waist of the participant. The data has been gathered using healthy human participants. The data was obtained from 17 participants, with different physical characteristics, and gender, and with an age range from 18 to 28. The Institutional Review Board at the California State University Long Beach approved the study protocol<sup>1</sup>

<sup>1</sup>IRB protocol number 639747-12

which conformed to the principles of the Declaration of Helsinki. All participants gave written informed consent before participation.

During the experiment (data acquisition), participants walked for 5 meters while wearing Walk-Even insoles on both feet. Data is recorded for each of the 12 sensors (6 on each foot) in pound-force (lbf) every 8ms (i.e. with a sampling rate of 125 Hz). Each data point is given a unique ID and a time step value. Hence, the 12 sensors generate a time series of pressure values. Each participant was recorded for 3 to 12 trials, totaling 108 valid trials. Moreover, the trials have different total lengths, in terms of time and therefore a different corresponding number of samples, as each participant walked the same distance but may have had different speeds and stride lengths.

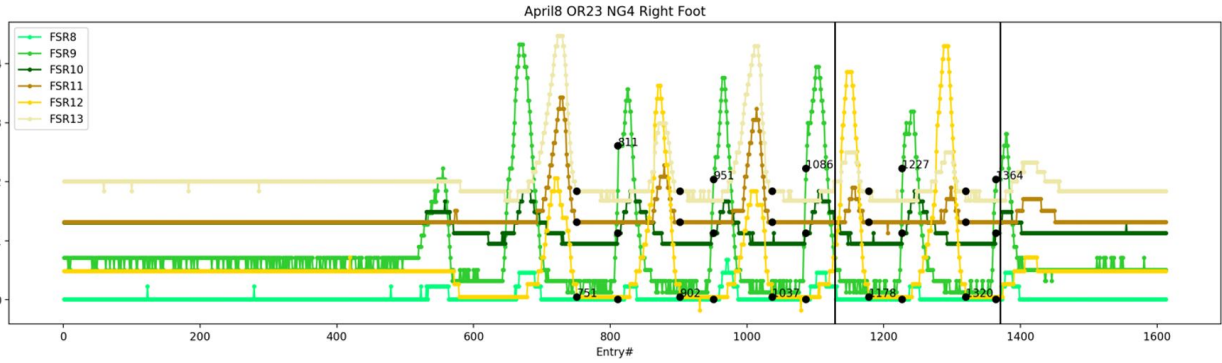


Figure 1: Example of a Trial: Plot of raw data values for each of six sensors on the right foot for participant NG.

Figure 1 shows a plot of raw data from one trial for participant NG. The plot shows the pressure value recorded for each sensor on the right foot. High values reported by force-sensitive resistive sensors (FSR) correspond to high pressure on the corresponding sensor when (a part of) the foot is on the ground, while low values correspond to the foot being in the air. Varying values of pressures are due to participant walking, thus shifting pressure from the back of the foot to the front, and due to placement of the sensors, being in the front, outer or inner edge, and back. In this study, we use pressure values for the right foot (six sensors) as inputs to the proposed deep learning models, during training and validation, as well as true data values (ground truth) during testing. We propose two distinct experimental setups, ‘by trial’ and ‘by participant’ that evaluate the model’s ability to make short-distance and long-distance predictions, respectively, the details of which are presented in 5.1.

## 4 Proposed Technique

### 4.1 Data Preprocessing

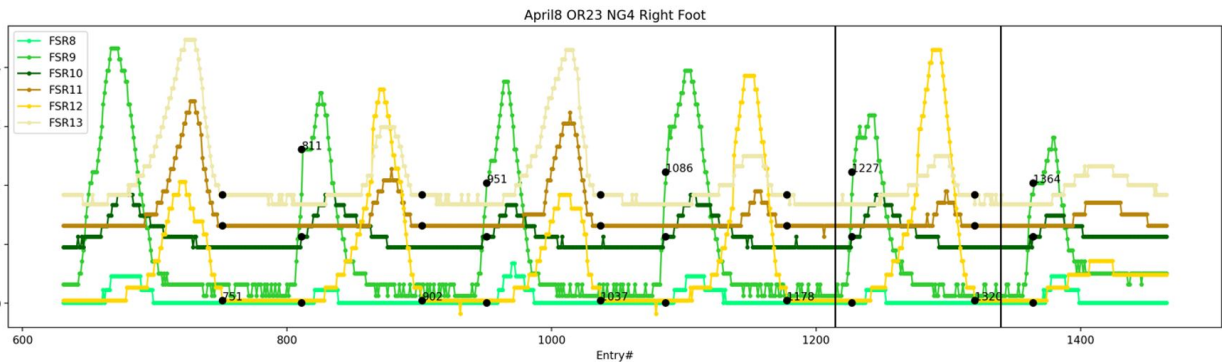


Figure 2: Example of a Trial: Plot of data values after preprocessing for each of six sensors on the right foot for participant NG.

As seen in Figure 1, the data on the far left-hand side (time steps less than 600) and on the far right-hand side (time steps greater than 1500) of the plot, do not match the swing or stance phase. This data corresponds to sensor readings

taken before and after the participant was instructed to walk, thus, this data should be removed. The preprocessing was done manually by careful visual observation of the plotted sensor values and their corresponding numerical values. We identified the time steps where the fluctuations in sensor data values start (for the beginning) and stop (for the end) to isolate the data values produced by walking. The resulting, truncated data is shown in Figure 2. The preprocessing ensures that data used to train, validate, and test the models represent true variations in sensor values that correspond to human gait.

Please note that the data supplied for training, validation, and testing has been windowed. For example, an input window of size 5 has values for 5 time steps for each of the sensors. Each input window is used to train and validate the model to predict one or more output values. The window size is selected for each experimental setup (please see 5.1). Additionally, the data is normalized based on the training data for that specific experiment (for the ‘by participant’ setup), meaning that an offset is added so that the minimum values are the same as for the training data. This is done for each trial to offset any differences between the trials and it serves instead of calibration.

## 4.2 Modeling

Recently, deep learning has been a significantly popular area among the machine learning and artificial intelligence community due to its improved learning capabilities Janiesch et al. [2021]. Thanks to convolutional neural networks (CNN) LeCun et al. [1998], Krizhevsky et al. [2012], Szegedy et al. [2015], Simonyan and Zisserman [2014] and recurrent neural networks (RNN) Kolen and Kremer [2001], Pascanu et al. [2013, 2012], Karpathy et al. [2015], deep learning architectures are implemented in various applications such as full self-driving system Ni et al. [2020], object detection Ren et al. [2015], He et al. [2017], machine translation Vaswani et al. [2017], and biomedical imaging analysis Zhang et al. [2021, 2015]. In this paper, we expand the application of several commonly used deep learning models to time-series gait data. We investigate the ability and quantify the accuracy of the customized models to predict different individuals’ walking patterns. Namely, we explore their capability to predict pressure values created by the participant at every time step. We implement and evaluate four different models of short- and long-distance prediction. The first three models are a variation of the RNN model, hence in the analysis we may refer to them as "RNN models" whereas the last one is an ensemble CNN and RNN model. The model description is given below.

*Recurrent Neural Networks (RNN)* Kolen and Kremer [2001] models are intensively implemented to recognize feature patterns in a sequential dataset. Most RNNs are used in time-series data, language-related data, or biological DNA sequence data. One key attribute of RNNs is the ability to work with varying lengths of input. RNNs were designed to capture the hidden state features by using recurrent computation at each time step. The RNN cell sums the dot product of the input and the weights with the dot product of the previous output and the corresponding weights then passes the data through an activation function. Since the parameters are shared during the whole training time, simple RNNs have suffered from vanishing gradient issues<sup>2</sup> especially if there is a long sequence of data, hence, the resulting model’s accuracy suffers.

*Long Short Term Memory (LSTM)* Hochreiter and Schmidhuber [1997] model refers to the RNN model with LSTM layers. The addition of LSTM cells helps alleviate the vanishing gradient problem. More precisely, the LSTM cells retain the input data, the previous cell’s hidden state, and the cell state. Consequently, the LSTM model has greatly increased computational complexity but generates more accurate predictions.

*Bidirectional LSTM (biLSTM)* Schuster and Paliwal [1997] model refers to an improvement of the LSTM model where the input has been considered in a forward direction and in a backward direction. Hence, the data is passed through two LSTM layers separately: one where the original input is utilized (forward direction) and another where the input is reversed (backward direction). The weights from the two LSTMs are concatenated (or combined using other specified functions), allowing the model to predict with a knowledge of what has happened prior and what will happen in the future. Therefore, this model, also, has further increased complexity and further improved accuracy.

*The (ensemble) CNN+RNN* model combines Convolutional Neural Network (CNN) and Recurrent Neural Network (RNN) models. CNN Krizhevsky et al. [2012], He et al. [2016] models are usually implemented for image classification problems due to the nature of convolutional layers. The convolutional layer, also known as the kernel or filter, performs a dot product of the input and the weights to help identify patterns in the input data (usually patterns in the images). Designing different CNN architectures by manipulating convolutional, pooling, and fully connected layers and varying respective parameters will allow specific features or patterns to develop from the input data. This is how the proposed CNN architecture is customized for this problem. CNN models has also been used on time-series data, but for successfully predicting stock market movement Liu et al. [2020] and forecasting stock prices Tsantekidis et al. [2017].

<sup>2</sup>Vanishing gradient issues arise in models with gradient-based learning methods, where the weights for the model are computed interactively using the partial derivative of the error function Basodi et al. [2020]. When the gradient becomes vanishingly small, it will prevent the weight from changing from iteration to iteration, or even completely stop the training of the neural network.

Tsantekidis et al. [2017] applied the CNN models, and Liu et al. [2020] used CNN and RNN for time-series data (separately, not as an ensemble model), motivating us to use it in the proposed ensemble model for time-series gait data values.

The intuition of combining CNN and RNN is that this model will fully address the vanishing gradient problem found in an RNN working with long sequences. Usually, CNN+RNN architectures are designed to deal with image captioning analysis but in this project, we leverage CNN+RNN architecture to preserve temporal features in long-distance gait data. Specifically, CNN is used to shorten the input data while maintaining the overall patterns, hence tackling the vanishing gradient problem. Working with temporal data sets, combining CNN and RNN has been shown to improve prediction outcomes while lowering computational costs compared to traditional RNN models. The CNN encodes the time-series features LeCun et al. [1998], then RNN decodes them to generate the next time-stamp sequences Shi et al. [2021]. The features extracted using CNN make for an excellent means to predict sequences of data such as translations, text generation, and time-series data, using RNN.

A concern when using a simple RNN for long sequences of data is the tendency for the first inputs used for training to have minimal to no effect on the outputs. Instead of using a simple RNN, one solution to this problem is to use a long short-term memory (LSTM) layer. The proposed method, CNN+RNN, consists of two 1-dimensional CNN layers and an RNN layer with LSTM cells to solve the information loss of long-distance sequential data.

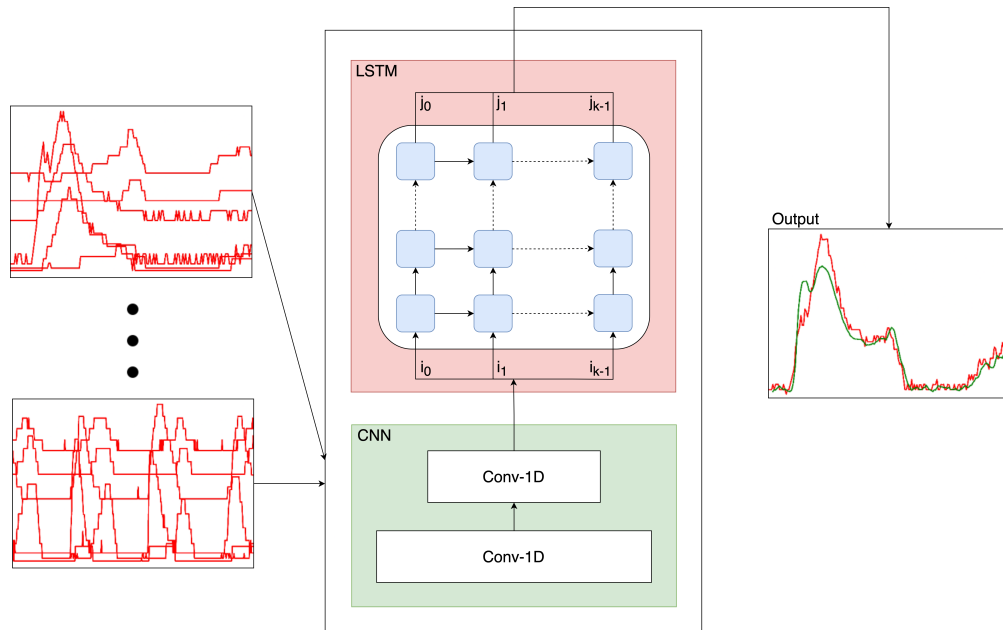


Figure 3: The proposed deep learning architectures, CNN+RNN, with two convolutional 1D layers (both with 20 filters each and kernel size 3), and one LSTM layer (with 20 units).

Figure 3 shows a block diagram of the proposed ensemble CNN+RNN model architecture when used for the setup ‘by participant’. On the left are examples of trials used as inputs: each plot shows time-series data for six sensor values for the duration of each trial. Even though the trials are shown separately, for the setup ‘by participant’ the trials are concatenated and windowed as they are provided as input. On the right is an example of the output: a plot of the sum of all six predicted values (shown in green) for one entire trial plotted alongside the sum of all six values of sensors’ reading, i.e. the true test data values (shown in red) for the same trial. The middle block represents the proposed custom model’s architecture that has been designed and fine-tuned on our dataset by experimentation. First, the input passes through the CNN section, composed of two 1-dimensional convolutional layers both of which have 20 filters with the kernel size set to 3. The output from this section is passed to the RNN, which is an LSTM layer with 20 units, followed by a dense layer<sup>3</sup>. Both convolutional layers in our proposed architecture have a kernel size of 3, which decreases the input, for example from 20 to 16. The LSTM layer takes these 16 data values as inputs and passes the outputs to the dense layer returning the prediction.

<sup>3</sup>The dense layer is not shown in Figure 3.

The proposed architecture is capable of predicting the entire trial. A predicted value is generated for each sensor (for each time step defined by the output window size). The evaluation metrics are computed for each data point, thus comparing the predicted values to true test data values for each sensor.

The model is also used in the ‘by trial’ setup. In this case, only a single trial is used as input. It is partitioned into the training and validation portions (for training), and a testing portion (to be compared to the predicted output, for testing).

### 4.3 Evaluation Metrics

To evaluate the performance of the several different deep learning models, we employ the commonly used metrics: Mean Absolute Error (MAE), Mean Squared Error (MSE), and Root Mean Squared Error (RMSE). The equations use  $y_i$  for the true test data value (i.e. the ground truth),  $\hat{y}_i$  for the predicted value, and  $N$  for the number of data values in the true test dataset.

MAE computes the average of the difference between the true test data values and predicted values through the dataset.

$$MAE = \frac{1}{N} \sum_{i=1}^N |\hat{y}_i - y_i| \quad (1)$$

MSE calculates the average of the squared difference between the true test data values and predicted values through the dataset.

$$MSE = \frac{1}{N} \sum_{i=1}^N (y_i - \hat{y}_i)^2 \quad (2)$$

RMSE is the square root of MSE.

$$RMSE = \sqrt{MSE} = \sqrt{\frac{1}{N} \sum_{i=1}^N (y_i - \hat{y}_i)^2} \quad (3)$$

MAE measures the average absolute distance from the prediction to the true test data values, MSE measures the vertical distance from the prediction to true test data values, and RMSE measures the variation between the predicted and true test data values. Therefore, we adopt *all three* measurements to evaluate the performance of our prediction models. A model with a *good fit* will have values *close to zero* for all three metrics. A model with the perfect fit will have them all equal to 0.

## 5 Experiments

### 5.1 Experimental Setup

We implement four deep learning models to predict sensor data values that correspond to an individual’s gait cycle: a simple RNN with a single RNN layer, an LSTM model with two LSTM layers, a Bidirectional LSTM (biLSTM) with two bidirectional LSTM layers, and the CNN+RNN model combining two 1-dimensional convolutional layers and an LSTM layer, as described in Section 4.2. The first three models are built on top of a simple RNN model, which we may refer to as RNN models in our analysis, and they are designed to predict short-distance sequential data. The last model (CNN+RNN) is designed to explore the ability to predict long-distance sequential data.

The proposed models are implemented in Keras 2.5.0 using the backend of Tensorflow 2.5.0 on the Google Cloud Platform with a two-core Intel Xeon CPU 2.30GHz. The optimizer for all RNN models is Adam Ada with a learning rate set to 0.0001, whereas the optimizer for the CNN+RNN model is RMSprop RMS with a learning rate set to 0.01. We also experimented with the use of dropout layers for all models. For all models, the first RNN layer used a recurrent dropout set to 0.5 and the CNN+RNN model used an additional dropout set to 0.1 for the LSTM layer. The use of a dropout layer produces results with inferior performance and hence we will not present them in the results section.

Typically, deep learning models are generated using a much larger number of features with very large training data sets. We face the challenge of having a smaller training set, containing 17 participants with 108 trials containing time-series sensor data for each of the six sensors, where each sensor value has been considered a feature. To overcome this challenge we carefully fine-tune model architectures and propose two different experimental setups: ‘by trial’ and ‘by participant’. Additionally, for every experiment, the data is normalized based on the training data for that specific experiment; this is especially pertinent for the setup ‘by participant’ due to the use of multiple trials for training,

Table 1: Time Parameters in Seconds for ‘by trial’ Setup: Average Training (and Validation) Time (Avg. Train), Average Prediction Time (Avg. Predict), Time to Generate True Test Data Values (Avg. Measured Test Time)

Model	Avg. Train Time [s]	Avg. Predict Time [s]	Avg. Measured Test Time [s]
Simple	84.157	0.084	
LSTM	175.310	0.084	
biLSTM	250.783	0.087	0.922
CNN+RNN	99.513	0.081	

validation, and testing. Both experimental setups use data values for the right foot (6 sensor values at each time step) as input data and predict 6 values corresponding to each sensor, at *one or more* consecutive (future) time steps.

The input data is being windowed, and each input window produces predictions for as many time steps as defined by the output size. The input and output window sizes are specified for each model, in two experimental setups. The input window size defines the number of time steps whose sensor values are used as inputs for generating the prediction. We vary the input size in two experimental setups. The output window size defines the number of time steps for which the prediction is generated. Each model contains a dense layer that makes  $6 \times W$  predictions, where 6 corresponds to each predicted sensor value, and  $W$  corresponds to the output window size. Two presented experimental setups have different values for the output window size. Since the ‘by trial’ experimental setup explores short-distance prediction, the output window size is 1, hence, the prediction will be made for one time step for each sensor value (a total of 6 predicted values). Since the ‘by participant’ experimental setup explores long-distance prediction, the output size is larger than 1. For example, when the output size is 3, the prediction will be made for three consecutive time steps, for each sensor value (a total of 18 predicted values). The predicted values for all sensors at each time step are summed, and graphed to easily compare the predicted values to (summed) true test data values. However, MAE, MSE, and RMSE values are computed using the predicted non-summed values and the true test data values.

### 5.1.1 Setup by Trial - Experimental Configuration

To explore the ability of all four models to perform short-distance prediction of sequential data this setup uses a single gait trial, split into approximately 70% for training, 15% for validation, and 15% for testing data. To ensure that testing and validation data would be 15% each, a function was created that allocated 15% of the input data plus the remainder final window size of data to the testing data, consequently making the training set equal to or set slightly below 70%. Figure 2 shows a truncated trial for participant NG. We show two black vertical lines towards the right side of the image (one to the right of time step 1200 and the other to the left of time step 1400) dividing the data into three segments. The largest segment to the left of the first black line corresponds to training data, the next segment corresponds to the validation, and the rightmost segment corresponds to the testing data set. If we were to compare the segments in Figure 2 to the original data shown in Figure 1 we see that the testing data would have contained mainly constant values, thus giving an unfair advantage to the evaluation of the model. This is one of the reasons to preprocess the data as in Section 4.1.

Since this setup targets short-distance prediction, the input window size is 5 and the output window size is 1. Training setup ‘by trial’ uses MSE as the loss function and trains for 40 epochs. All models for setup ‘by trial’ are capable of predicting the data in under one-tenth of value generation time (using true test data values). Table 1 shows average values of time parameters for our experiments ‘by trial’, reported in seconds. The average training (and validation) time for all models spans between 84 and 251 sec, showing that the customized models take a very short time to train (below 5 min for the most complex one). As expected, Simple RNN has the shortest, while biLSTM has the longest training time. Our custom CNN+RNN architecture trains, on average, for 99.5 sec, which is just slightly longer compared to the training time of the simple RNN. Average prediction times are between 0.081 sec (CNN+RNN) and 0.084 sec (Simple RNN and LSTM). Similar to training, biLSTM takes the most time to predict (0.087 sec). Additionally, the average time a participant takes to walk the distance that corresponds to the testing portion of the trial (thus generating true test data values) is 0.922 sec. We see that all models are *able to predict the values in real-time*, and the prediction time is more than ten (10) times shorter than the data generation/acquisition.

### 5.1.2 Setup by Participant - Experimental Configuration

To explore the ability of all four models to perform long-distance prediction of sequential data, we introduce a second experimental setup that evaluates the different input and output window sizes for each participant, for all proposed deep learning models. For this experimental setup, one trial was allocated for testing, another for validation, and the remaining trials were first windowed and then concatenated together to form the training data set. The window size has

Table 2: Time Parameters in Seconds for 'by participant' Setup: Average Training (and Validation) Time (Avg. Train), Average Prediction Time (Avg. Predict), Time to Generate True Test Data Values (Avg. Measured Test Time)

Model	Avg. Train Time [s]	Avg. Predict Time [s]	Avg. Measured Test Time [s]
Simple	61.302	0.082	
LSTM	153.448	0.101	
biLSTM	265.008	0.111	57.870
CNN+RNN	94.352	0.088	

an input size of 5, 10, 15, and 20 and an output size of 3, 4, and 5 for each input size. For each participant and for each model we explore a total of 12 input/output combinations (4 input and 3 output values). Training setup 'by participant' uses MAE as the loss function and trains for 20 epochs.

All models in this setup are capable of predicting all true test data values for the entire trial within 0.12 seconds. Table 2 shows average values of time parameters for our experiments 'by participant', reported in seconds. The average training (and validation) time for all models spans between 62 and 265 sec, showing that the customized models, even for the long-distance prediction take a very short time to train, which is comparable to the time taken to train 'by trial' models. As expected, Simple RNN has the shortest, while biLSTM has the longest training time. Our custom CNN+RNN architecture trains, on average, for 94.4 sec, which is about 50% longer compared to the training time of the simple RNN. Average prediction times are between 0.082 sec (Simple RNN) and 0.111 sec (biLSTM). As expected, biLSTM takes the most time to predict (0.111 sec) and CNN+RNN takes close to the minimum time (0.088 sec). Additionally, the average time a participant takes to walk the distance that corresponds to test trial (thus generating true test data values) is 57.870 sec. We see that all models are *able to predict the values in real-time*, and the prediction time is a small fraction of the time of the data generation/acquisition.

Please note that the 'by participant' setup predicts the entire trial and, within it, values for each sensor at *multiple* time steps, whereas the 'by trial' setup predicts only 15% of a trial and within it a single value for each sensor at *one* time step. Therefore, CNN+RNN is shown to be faster than other models while predicting more accurately a larger amount of values than other models.

### 5.1.3 Participant Selection

Our current gait data are produced with healthy participants and we run experiments for both setups for all trials from all participants. This means that the 'by trial' setup uses all 108 trials separately for a total of 108 experiments. Additionally, the 'by participant' setup uses 108 trials that are combined into 17 groups, one for each participant. Moreover, it runs experiments for each input and output window combination for a total of 204 experiments. Due to space limitations, we present aggregated data for each setup and only a subset of experiments showcasing the trials and participants that illustrate experiments that are closest to presented averages, the best-performing and the poorest-performing models. We also present trials and participants that give us some insight into the used model and experimental setup, or showcase lessons learned for the future. Hence, the trials and participants that we present were selected solely to show the results that illustrate our findings for each setup.

## 5.2 Results, Analysis, and Discussion

We present and compare the experimental results and visualization for predicting force-resistive sensor data values for the setups 'by trial' and 'by participant'. In the tables, we display the values of each evaluation metric for each model. We indicate the performance of the model by shading from dark green (best) to pale yellow (poorest). The graphs show the summed sensor values, and, as needed, individual sensor values for the true test data values and the predicted data values. In both types of graphs, the true test data values (i.e. the sensor readings) are shown in blue and the predicted values are shown in pink. The graphs that plot (raw) sensor data, which show separate values for each force-sensitive resistive sensor (FSR 8 -13), are added to aid the analysis of training and prediction. The type of graph presented for each experiment was selected to facilitate an understanding of the model's ability or obstacles while making accurate predictions.

### 5.2.1 Setup by Trial

The average scores for all three metrics, and a median value for RMSE of all models for 'by trial' are presented in Table 3. The values are computed per participant, where each participant is identified by a two-letter code in front of each model and had multiple (3 to 12) trials. The numerical values for RMSE show that biLSTM model performs the best of

	AVG_MAE	AVG_MSE	AVG_RMSE	MED_RMSE		AVG_MAE	AVG_MSE	AVG_RMSE	MED_RMSE
NS Simple	0.075649	0.011342	0.104451	0.093373	NB Simple	0.128121	0.038626	0.179959	0.164901
NS LSTM	0.075356	0.010651	0.102655	0.098466	NB LSTM	0.126015	0.042960	0.189401	0.152600
NS biLSTM	0.063972	0.007865	0.088383	0.085650	NB biLSTM	0.122139	0.037792	0.177848	0.138604
NS CNN+RNN	0.108961	0.024579	0.153617	0.154832	NB CNN+RNN	0.171552	0.064510	0.240346	0.220390
JM Simple	0.055569	0.007151	0.083442	0.077392	AM Simple	0.070904	0.009726	0.098063	0.093510
JM LSTM	0.055829	0.007830	0.086673	0.078818	AM LSTM	0.070573	0.010447	0.101573	0.097976
JM biLSTM	0.050014	0.006210	0.077436	0.073192	AM biLSTM	0.062925	0.008640	0.092371	0.092829
JM CNN+RNN	0.074205	0.013909	0.115494	0.109386	AM CNN+RNN	0.090835	0.018913	0.136368	0.133798
JG Simple	0.104448	0.029630	0.152807	0.111839	AJ Simple	0.110288	0.024309	0.150483	0.151583
JG LSTM	0.093916	0.019479	0.131707	0.107060	AJ LSTM	0.117432	0.030432	0.168242	0.164283
JG biLSTM	0.078617	0.014959	0.117426	0.101079	AJ biLSTM	0.098734	0.021964	0.144186	0.139000
JG CNN+RNN	0.123160	0.039212	0.192344	0.181019	AJ CNN+RNN	0.136390	0.044484	0.203672	0.193148
OB Simple	0.095066	0.021913	0.142776	0.128266	CD Simple	0.126818	0.046416	0.201329	0.199304
OB LSTM	0.087220	0.022479	0.143475	0.132414	CD LSTM	0.139045	0.054151	0.214759	0.226506
OB biLSTM	0.072956	0.015994	0.119973	0.102530	CD biLSTM	0.132663	0.053621	0.210149	0.202250
OB CNN+RNN	0.103571	0.028783	0.165620	0.154657	CD CNN+RNN	0.156870	0.065352	0.242739	0.227154
RL Simple	0.078809	0.012695	0.112179	0.117556	JP Simple	0.095625	0.019746	0.136161	0.121144
RL LSTM	0.085345	0.016483	0.123728	0.111004	JP LSTM	0.109143	0.027369	0.156844	0.137153
RL biLSTM	0.076309	0.012239	0.108217	0.101467	JP biLSTM	0.082140	0.015729	0.121501	0.115969
RL CNN+RNN	0.112963	0.026655	0.162162	0.172310	JP CNN+RNN	0.147602	0.052723	0.220888	0.205809
RR Simple	0.069538	0.012332	0.105103	0.104386	OR Simple	0.094933	0.023278	0.142541	0.122753
RR LSTM	0.066261	0.012015	0.105455	0.107752	OR LSTM	0.094866	0.023213	0.143696	0.120737
RR biLSTM	0.057485	0.009177	0.093306	0.097054	OR biLSTM	0.086557	0.017639	0.128905	0.119717
RR CNN+RNN	0.081901	0.017748	0.131033	0.121654	OR CNN+RNN	0.122168	0.038980	0.180979	0.148495
CR Simple	0.101394	0.023526	0.149811	0.158139	SY Simple	0.096279	0.023250	0.151387	0.150256
CR LSTM	0.120047	0.033615	0.178890	0.192764	SY LSTM	0.101713	0.026723	0.162652	0.161068
CR biLSTM	0.102909	0.025442	0.155249	0.168124	SY biLSTM	0.087286	0.018984	0.136248	0.139990
CR CNN+RNN	0.162884	0.069540	0.257155	0.236444	SY CNN+RNN	0.141123	0.049143	0.215673	0.213121
AR Simple	0.073484	0.011840	0.107450	0.101809	KL Simple	0.069331	0.014779	0.121396	0.124403
AR LSTM	0.066180	0.011662	0.106256	0.103266	KL LSTM	0.070241	0.016208	0.127296	0.126763
AR biLSTM	0.057023	0.008973	0.094652	0.094859	KL biLSTM	0.062600	0.012352	0.110846	0.109696
AR CNN+RNN	0.103442	0.025365	0.159079	0.160004	KL CNN+RNN	0.093197	0.028163	0.166115	0.159165
EJ Simple	0.102318	0.021316	0.144844	0.153706					
EJ LSTM	0.102626	0.024949	0.157360	0.161359					
EJ biLSTM	0.088664	0.019383	0.137182	0.139685					
EJ CNN+RNN	0.139983	0.045525	0.210701	0.201122					

Table 3: Setup by Trial: Average Error Metrics by Model

all four models on average. Additionally, it is the best-performing model for most of the trials (69 out of 108 trials), when the results for each trial are observed separately. The worst-performing model, on average, is the CNN+RNN.

We present below three trials that give us insight into the performance of the ‘by trial’ experimental setup.

**Trial 1 by Participant RR** The results for this trial follow a similar trend to the experiment’s overall average, where the biLSTM models perform the best, followed by RNN, LSTM, and lastly, CNN+RNN. Table 4 shows the numerical error values for a trial from participant RR (referred to as Trial 1 - RR).

This trial, at face value, is the best performing amongst all the experiments in setup ‘by trial,’ with the lowest RMSE score of 0.060675 for the biLSTM model. Other RNN models show comparable performance, while the CNN+RNN has a noticeable struggle with prediction accuracy, showing a much higher RMSE value than the other three models. The plots of true test data values and predicted values (Figures 4 a) - d)) clearly show this observation. Figures 4 a) - c) visualize the better performance of the RNN models (RNN, LSTM, and biLSTM) compared to the CNN+RNN model shown in Figure 4 d). The CNN+RNN shows a much larger difference between the true test data values and

Trial 1 - RR	MAE	MSE	RMSE
Simple	0.043110	0.003790	0.061561
LSTM	0.038233	0.003795	0.061607
biLSTM	0.034449	0.003681	0.060675
CNN+RNN	0.088238	0.022798	0.150990

Table 4: Setup by Trial: Trial 1 - RR Error Metrics

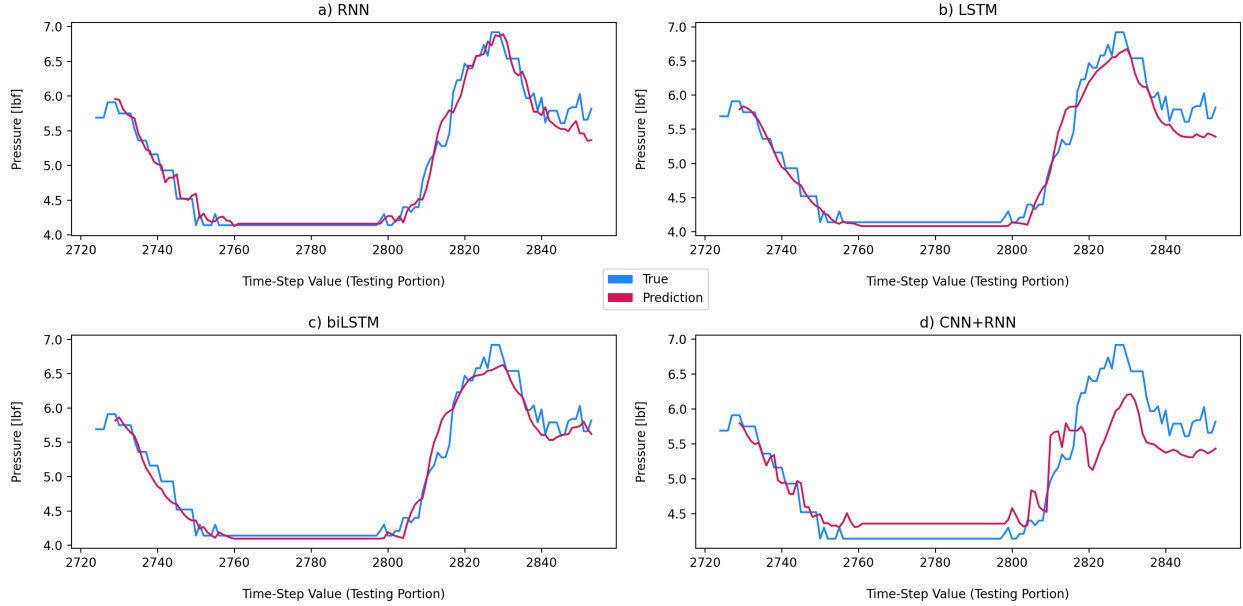


Figure 4: Setup by Trial: Trial 1 - RR Summed up Values for all (Sensors) True Test Data Values (blue) vs Predicted Data Values (red)

the prediction data values compared to the RNN models (RNN, LSTM, and biLSTM). Visual inspection of raw data values (plot not included here) shows that two of the sensors experience significantly smaller variations in the testing portion of the truncated data than in the training/validation portion of the data. Hence, the pattern during testing is much different than the established pattern during the training and validation, which prevents CNN+RNN from more accurate predictions.

Trial 2 - AJ	MAE	MSE	RMSE
Simple	0.139809	0.033077	0.181871
LSTM	0.178423	0.067618	0.260035
biLSTM	0.131149	0.033742	0.183691
CNN+RNN	0.210185	0.090216	0.300360

Table 5: Setup by Trial: Trial 2 - AJ Error Metrics

**Trial 2 by Participant AJ** Table 5 shows the numerical error values for one trial from participant AJ (referred to as Trial 2 - AJ). This trial tests the adaptability of all the models to predict data that greatly differs from the training input. To explore the behavior of all models under these circumstances, we look into the truncated data for the individual sensors shown in Figure 5. The fluctuation of the values in the training or validation datasets for FSR 9 are vastly different from the fluctuations in the testing portion. Moreover, for FSR 8, FRS 10, and FSR 11 the values for the testing dataset also slightly differ from the training and validation sets. Figure 6. shows separately plotted true test data values (blue) and predicted values (pink) for each sensor, where the values for FSR9 have been highlighted using solid

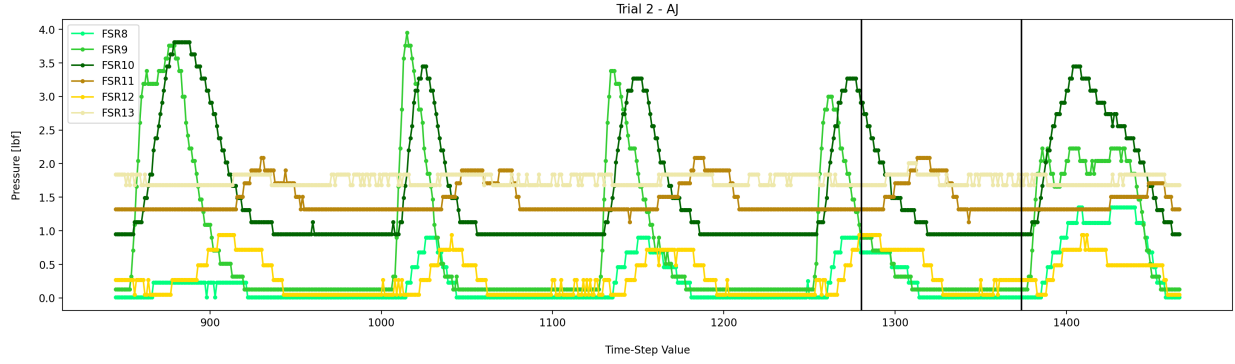


Figure 5: Setup by Trial: Trial 2 - AJ

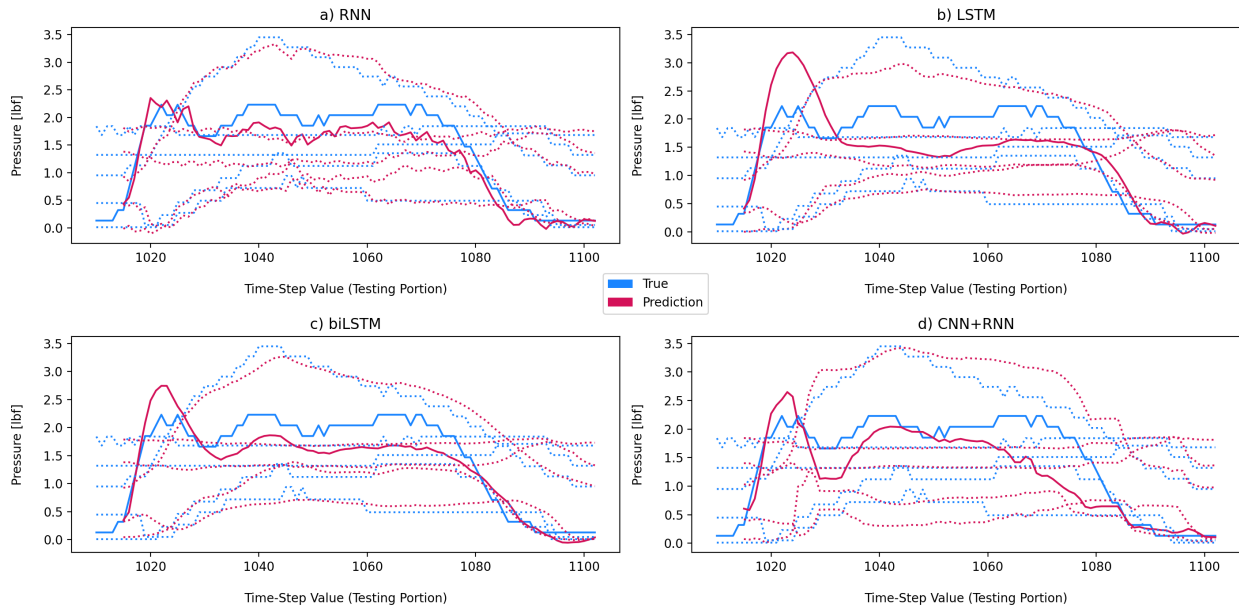


Figure 6: Setup by Trial: Trial 2 - AJ Individual Values for all (Sensors) True Test Data Values (blue) vs Predicted Data Values (red)

lines. The predicted values for all models do not follow closely the true test data values. The difference in patterns of training and validation data compared to true test data values (Figure 5) gives insight into poor performance. This trial underlines the setbacks for the CNN+RNN and the advantages of the RNN models (specifically the RNN and biLSTM models). The RNN and biLSTM models perform adequately at predicting the true test data values. The separately plotted data in Figure 6 shows that both models struggle at correctly predicting FSR 9 but to some extent capture the overall trend of the rest of the sensor data. The CNN+RNN, on the other hand, struggles with predicting the values for most of the sensors.

Trial 3 - AJ	MAE	MSE	RMSE
Simple	0.075109	0.011365	0.106609
LSTM	0.114885	0.026989	0.164283
biLSTM	0.090120	0.019321	0.139000
CNN+RNN	0.122461	0.037306	0.193148

Table 6: Setup by Trial: Trial 3 - AJ Error Metrics

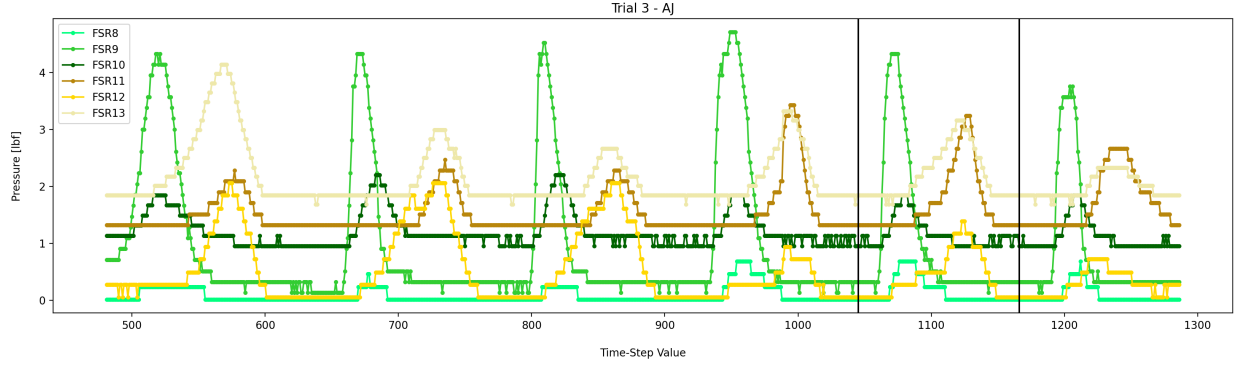


Figure 7: Setup by Trial: Trial 3 - AJ

**Trial 3 by Participant AJ** Table 6 shows the numerical error values for the last trial presented in this experimental setup, another (different) trial from participant AJ (referred to as Trial 3 - AJ). In this trial, the simple RNN outperforms all models, and the CNN+RNN (expectantly) performs poorly. As seen in Figure 7 the last (testing) segment of data has a significantly different pattern than the training data. In this trial, FSR 9 and FSR 11 have vastly different values during testing from the corresponding values in training. We need to be cognizant of the applications of our method. The models will likely have much better performance if the true test data is allocated from a segment that corresponds to the established rhythm of walking, and not from the end/slowdown, where the walking pattern differs.

This observation points to another direction for future experimental work: we might be able to use the value of RMSE as an indicator of change of pattern for the participant within a single trial. We would train the models with the data collected at the beginning of walking, hence, we would capture the established pattern. As a participant walks for a longer time, they might experience fatigue, and therefore a change of pattern. The change of pattern could be detected and its quantitative measurement (RMSE) could be reported. This application would be suitable for evaluation and recovery monitoring.

*Discussion:* The trials in our dataset are comprised of varying recorded lengths of time when an individual walks. After truncating the data to ensure the initial and concluding readings were removed (please see Section 4.1), the length of data for each trial varied even further. The longer the trial, the more data was allocated for each portion: training, validation, and testing. As a result of having more data in the testing dataset, there is a chance for the testing dataset to be comprised of a swing phase along with a stance phase. During the swing phase of the gait cycle, the sensors are not in contact with the ground, resulting in relatively flat (small) sensor values. These relatively flat values are easy for the models to predict, which will favorably influence the RMSE and other error metrics. With smaller trials, and, thus, smaller testing portions, there is less chance of a swing phase to be included in the testing portion, which may lead to that model performing much worse in comparison to the longer trials. Trial 1 - RR is one such example where the testing portion includes a swing phase. Additionally, we trained the model on the data that corresponds to the beginning, validated the data towards the end, and tested it at the very end of the trial. The implications are that the training and validation were done when the participant had established a rhythm during walking. However, the testing is done as they are slowing to a stop. Therefore, the pattern of walking corresponding to the testing data may differ from the pattern for the data corresponding to training and validation, sometimes having fewer changes in data values. Using Figure 4 d) we can observe that the CNN+RNN model does not perform well during the stance phases, and the swing phase of the prediction is likely helping to reduce the error metrics. With this in mind, it is important to note that the RMSE and other error metric scores, while indicative of accuracy for a specific trial, should not be the only means to compare prediction accuracy from different trials. A swing phase, which is a natural part of the gait cycle, may be included in the test portion of one but not in the test portion of another trial, thus resulting in a smaller RMSE for the trial whose true test data values include the swing phase. The accuracy of prediction for the ‘by trial’ setup will depend on the inclusion of the swing or stance phase in testing data.

We can make a few general observations: the CNN+RNN model may be less capable at short-distance prediction when the pattern in testing is slightly different than the pattern learned from training, and all models have an ‘advantage’ at predicting when the data in the true test dataset has fewer fluctuations (swing phase). Nevertheless, the RNN, LSTM, and biLSTM models show very good accuracy for short-distance prediction for the data where the values of the training dataset vary in a slightly different way than in testing (Figure 4 a) - c)). This observation motivates our future work, where we would like to explore detecting pattern changes for non-healthy participants while walking. One idea is developing a deep-learning model to detect changes from the established pattern in real-time, by means of increasing

errors between the predicted and newly generated data (corresponding to the testing portion). To peruse this line of work we need to evaluate the prediction run-time (please see Section 6) and carefully consider short- vs. long-distance prediction capabilities.

Overall, the short-distance prediction using RNN models shows promising results and warns us of the importance of data capturing during experimentation in the (physical) laboratory environment and the selection of training, validation, and testing datasets during modeling and testing.

### 5.2.2 Setup by Participant

	AVG_MAE	AVG_MSE	AVG_RMSE	MED_RMSE		AVG_MAE	AVG_MSE	AVG_RMSE	MED_RMSE
Simple 5-3	0.138692	0.063852	0.245637	0.248294	Simple 15-3	0.133437	0.061189	0.233143	0.212135
LSTM 5-3	0.133903	0.062739	0.244199	0.247582	LSTM 15-3	0.133629	0.062950	0.238802	0.226607
biLSTM 5-3	0.111697	0.044461	0.206854	0.206648	biLSTM 15-3	0.116965	0.048491	0.209360	0.187729
CNN+RNN 5-3	0.125808	0.050973	0.221024	0.215513	CNN+RNN 15-3	0.122905	0.052908	0.221101	0.194171
Simple 5-4	0.166647	0.098617	0.300340	0.283082	Simple 15-4	0.169865	0.105226	0.309171	0.309320
LSTM 5-4	0.161648	0.094924	0.294797	0.272993	LSTM 15-4	0.170828	0.107559	0.312558	0.313391
biLSTM 5-4	0.129987	0.067683	0.248877	0.242931	biLSTM 15-4	0.141262	0.079929	0.270259	0.285585
CNN+RNN 5-4	0.139390	0.070288	0.256660	0.250392	CNN+RNN 15-4	0.140950	0.076592	0.266080	0.281764
Simple 5-5	0.186553	0.122427	0.332501	0.347840	Simple 15-5	0.189160	0.130088	0.339874	0.358067
LSTM 5-5	0.183073	0.126364	0.337522	0.368283	LSTM 15-5	0.182949	0.122474	0.334327	0.374449
biLSTM 5-5	0.144551	0.083201	0.274123	0.268770	biLSTM 15-5	0.153518	0.088877	0.283633	0.278946
CNN+RNN 5-5	0.142918	0.078332	0.267497	0.247384	CNN+RNN 15-5	0.141719	0.075543	0.261884	0.242301
Simple 10-3	0.134352	0.063353	0.236969	0.272742	Simple 20-3	0.134776	0.059585	0.238807	0.236384
LSTM 10-3	0.130869	0.062115	0.235395	0.272337	LSTM 20-3	0.138894	0.064434	0.248001	0.256029
biLSTM 10-3	0.111820	0.048581	0.208373	0.205602	biLSTM 20-3	0.127244	0.055018	0.229279	0.244324
CNN+RNN 10-3	0.121094	0.051924	0.219891	0.216242	CNN+RNN 20-3	0.116947	0.048331	0.216047	0.213850
Simple 10-4	0.163807	0.093475	0.289282	0.301143	Simple 20-4	0.168345	0.100237	0.299989	0.305900
LSTM 10-4	0.156203	0.088527	0.286165	0.297492	LSTM 20-4	0.174248	0.106861	0.311728	0.328108
biLSTM 10-4	0.130030	0.061892	0.239126	0.241836	biLSTM 20-4	0.144838	0.079891	0.269986	0.274158
CNN+RNN 10-4	0.136317	0.066828	0.247336	0.238140	CNN+RNN 20-4	0.131804	0.065532	0.246040	0.238203
Simple 10-5	0.191007	0.128441	0.339574	0.366402	Simple 20-5	0.187320	0.123410	0.333965	0.367619
LSTM 10-5	0.179889	0.118405	0.329098	0.352326	LSTM 20-5	0.189006	0.126673	0.339506	0.397289
biLSTM 10-5	0.150520	0.086569	0.280593	0.283071	biLSTM 20-5	0.163954	0.099327	0.301494	0.315407
CNN+RNN 10-5	0.143632	0.078074	0.266303	0.248721	CNN+RNN 20-5	0.146974	0.079762	0.270186	0.267861

Table 7: Setup by Participant: Average Error Metrics by Model

The average values for all 3 metrics for each experiment in the ‘by participant’ setup while varying window size for both input and output (prediction) are shown in Table 7. The input window size takes a value from a set (5, 10, 15, 20) and an output window from a set (3, 4, 5) for each input size, thus forming a total of 12 combinations for each participant and for each model. We also calculate and present the median value for RMSE as this experiment compares results for prediction for different participants. The tables follow the same shading scheme (dark green - best, pale yellow - poorest), and in addition, the outline shows the best, and lowest values for average and median values for RMSE, respectively.

The numerical results indicate that for smaller input window sizes, 5-3, 5-4, 10-3, 10-4, and 15-3, the biLSTM model performs the best. However, for all other, larger, input window sizes the CNN+RNN models perform the best. These results align with the intuition behind the models. The biLSTM uses all input data to formulate the prediction, and therefore it performs very well for small window sizes. In the CNN+RNN model, the convolutional layers decrease the size of the input data by passing the data through filters while keeping the information pertinent to the prediction. Conversely, with larger input windows, the convolutional layers can extract the pattern much faster and easier while discarding the excess data, hence showing better performance. The RNN models do not have this capability. With the larger window sizes the biLSTM and the other RNN models, struggle with the increased input data size, while the CNN+RNN excels. We present the results for a total of six participants: the first four (Tables 8 - 11) present the best result for each of the considered input sizes, where the output size is selected based on the best RMSE score for CNN+RNN model. The next participant is selected to showcase an outlier: a case where biLSTM outperforms

CNN+RNN by a small margin (Table 12). The last participant included a set of results (Tables 13) illustrating how much better the CNN+RNN model performs for larger inputs compared to the RNN models.

NS 5-5	MAE	MSE	RMSE
Simple	0.239719	0.141073	0.375596
LSTM	0.202377	0.107894	0.328472
biLSTM	0.148915	0.062290	0.249580
CNN RNN	0.106307	0.034352	0.185342

Table 8: Setup by Participant: NS 5-5 Error Metrics

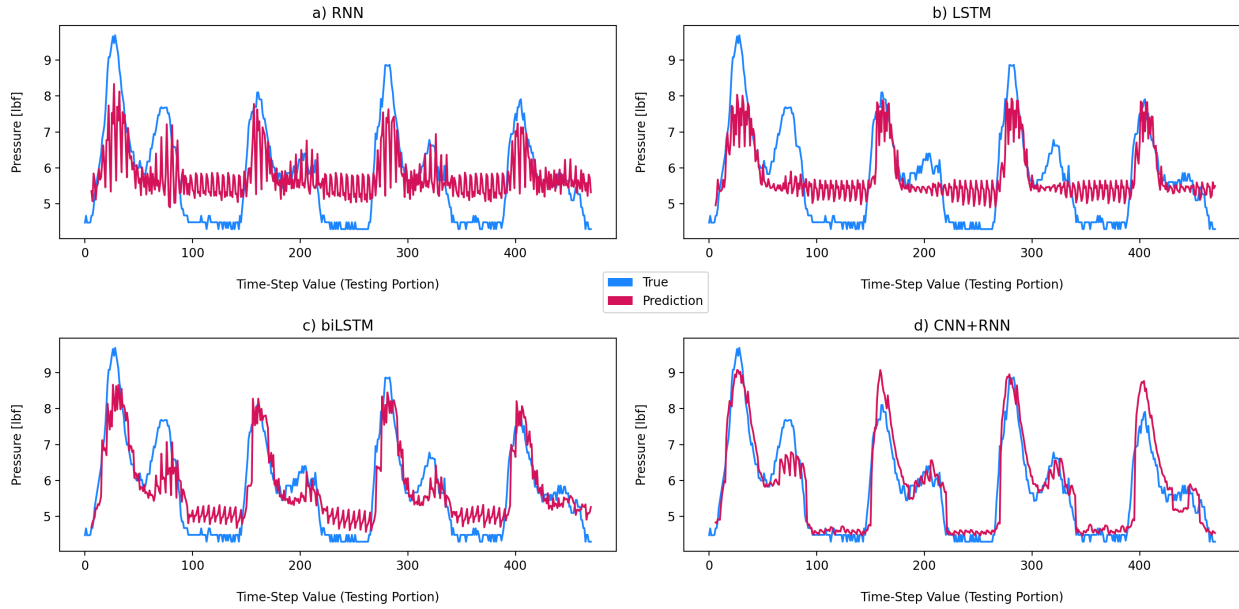


Figure 8: Setup by Participant: NS 5-5 Summed up Values for all (Sensors) True Test Data Values (blue) vs Predicted Data Values (red)

**Participant NS 5-5** Table 8 shows the numerical error values for participant NS for input window value of 5 and output window value of 5 (referred to as NS 5-5), the participant with best performing CNN+RNN 5-5 model. For a short input, the intuition would be that the CNN+RNN would suffer due to a lack of input data. However, based on the average values, the CNN+RNN model performs best for this window for the large majority of participants for 5-5 experiments. All three RNN models underperform compared to CNN+RNN. We argue that while the input window is considerably small (i.e. manageable for RNN models), the large output window (5) in combination with the small input window makes it difficult for the RNN models to accurately predict. The sum of true test data values (sensor values) and predicted data values are shown in Figures 8.a) - 8.d) for the four observed models for NS 5-5. The cause for the large values for RMSE for the RNN and LSTM models is clearly visible in Figures 8 a) and b) as a miss-match between true test and predicted data values. The prediction with the smaller values of RMSE shows a much better fit as seen in Figures 8.c) and 8.d), with CNN+RNN (Figures 8.d)) being the most accurate.

**Participant JM 10-3** Table 9 shows the numerical error values for participant JM for an input window value of 10 and output window value of 3 (referred to as JM 10-3). This set of results is from the best-performing participant JM (best overall performance for all participants and all input/output window sizes) and shows that each of the models performs similarly well, with the CNN+RNN model performing slightly worse than the RNN models (RMSE for CNN+RNN model is by 0.018742 greater than RMSE for the best-performing model biLSTM). CNN+RNN does not exhibit its usual best performance. For this participant, the CNN+RNN performance is slightly worse than other RNN models, as the output size is fairly small (3 rather than 5) for CNN+RNN to be efficient. Figures 9.a) - 9.d) show that the prediction

JM 10-3	MAE	MSE	RMSE
Simple	0.058290	0.008237	0.090755
LSTM	0.061849	0.009831	0.099150
biLSTM	0.054362	0.007678	0.087623
CNN RNN	0.067966	0.011313	0.106365

Table 9: Setup by Participant: JM 10-3 Error Metrics

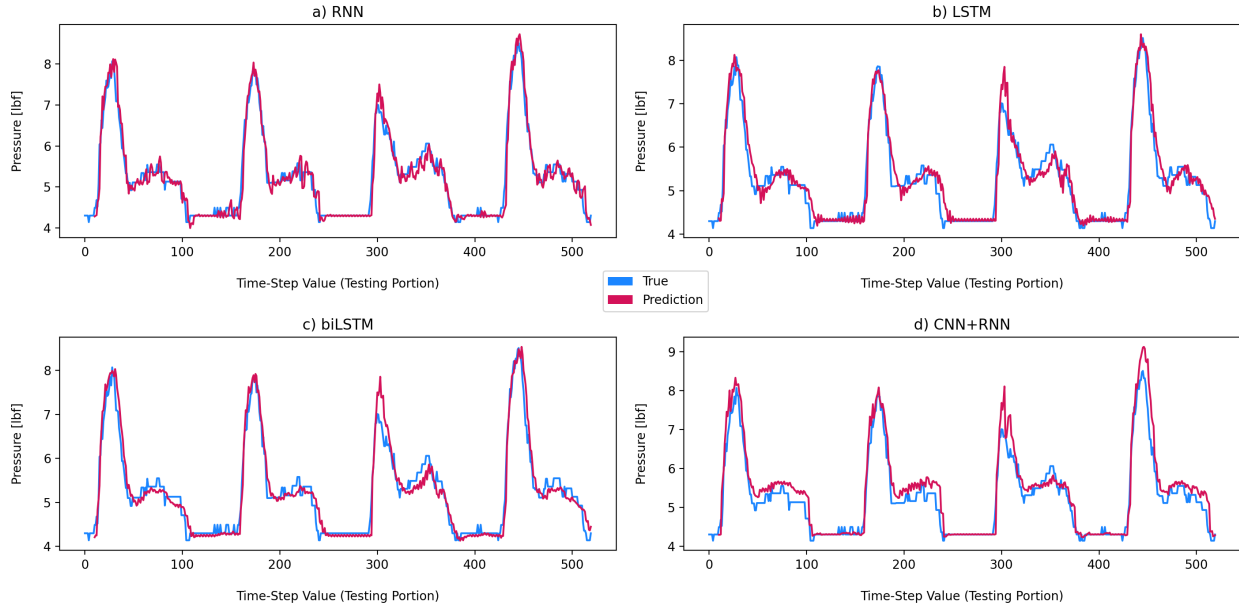


Figure 9: Setup by Participant: JM 10-3 Summed up Values for all (Sensors) True Test Data Values (blue) vs Predicted Data Values (red)

closely follows the true test data values for all models. biLSTM is the best-performing model for this participant in input/output window size (Figure 9.c).

In general, all four models for JM 10-3 perform better than previous models for participant NS (NS 5-5). Specifically, the CNN+RNN model for JM 10-3 performs better than all models for participant NS 5 - 5 due to increased input window size: from 5 (for NS 5-5) to 10 (for JM 10-3).

NS 15-4	MAE	MSE	RMSE
Simple	0.196944	0.095679	0.309320
LSTM	0.189772	0.090867	0.301442
biLSTM	0.138065	0.045745	0.213881
CNN+RNN	0.093105	0.028607	0.169135

Table 10: Setup by Participant: NS 15-4 Error Metrics

**Participant NS 15-4** Table 10 shows the numerical error values for participant NS for an input window value of 15 and an output window value of 4 (referred to as NS 15-4). This is the participant that has the best-performing model for the input size of 15. The smallest RMSE is obtained for the CNN+RNN model, and this model significantly outperforms all other RNN models. The input window size is large, making it difficult for RNN models to generate accurate predictions. Although CNN+RNN is the best-performing model, its RMSE is slightly larger than for JM 10-3.

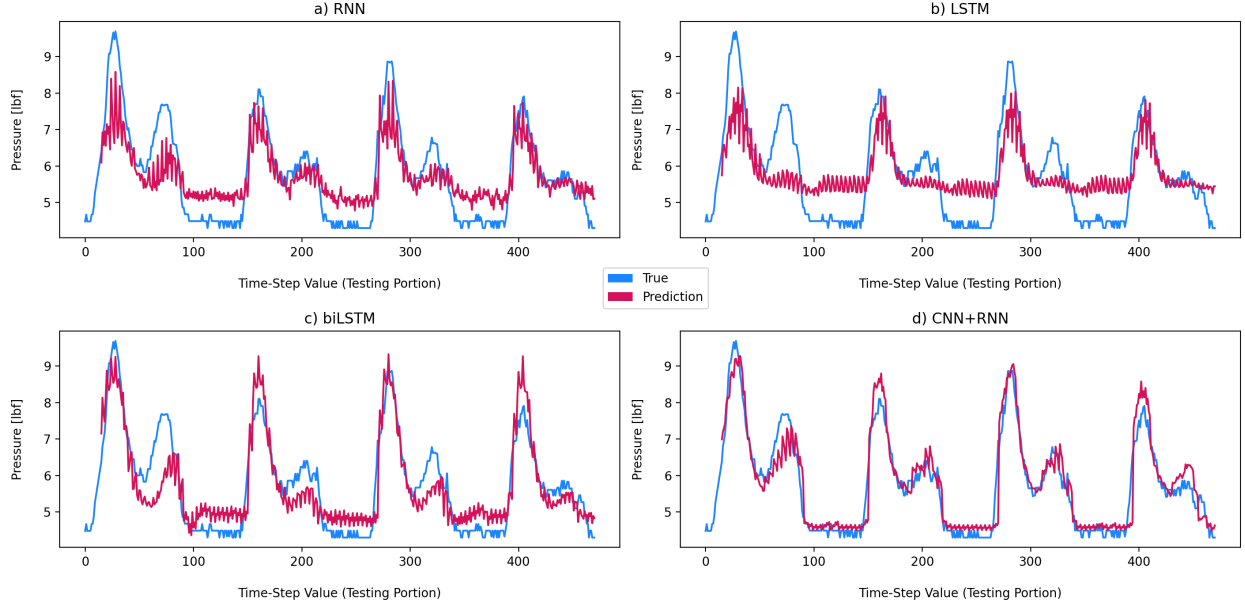


Figure 10: Setup by Participant: NS 15-4 Summed up Values for all (Sensors) True Test Data Values (blue) vs Predicted Data Values (red)

We hypothesize that the input size of 15 is not sufficient for accurate prediction for 4 consecutive values. Figures 10.a) - 10.d) visualize the prediction values for all 4 models. We can observe a better fit for CNN+RNN prediction compared to RNN predictions. Additionally, the visualization confirms the slightly poorer performance of all models compared to the models for JM 10-3.

JM 20-3	MAE	MSE	RMSE
Simple	0.077237	0.016850	0.129806
LSTM	0.083051	0.020695	0.143856
biLSTM	0.074897	0.018159	0.134755
CNN RNN	0.066030	0.013731	0.117179

Table 11: Setup by Participant: JM 20-3 Error Metrics

**Participant JM 20-3** Table 11 shows the numerical error values for participant JM for an input window value of 20 and output window value of 3 (referred to as JM 20-3). Because the input window is so large, the CNN+RNN does a great job at finding patterns in the data, leading it to perform the best even with the small output window. At the same time, the input size becomes too large for RNN models to generate accurate predictions. The RNN models have slightly higher values of RMSE compared to the values for JM 10-3. Figures 11.a) - 11.d) visualize the prediction values for all 4 models. They show a noticeably better fit for CNN+RNN prediction compared to RNN predictions.

JM 20-5	MAE	MSE	RMSE
Simple	0.084778	0.016954	0.130208
LSTM	0.092913	0.020086	0.141726
biLSTM	0.070232	0.013905	0.117921
CNN RNN	0.072060	0.015099	0.122878

Table 12: Setup by Participant: JM 20-5 Error Metrics

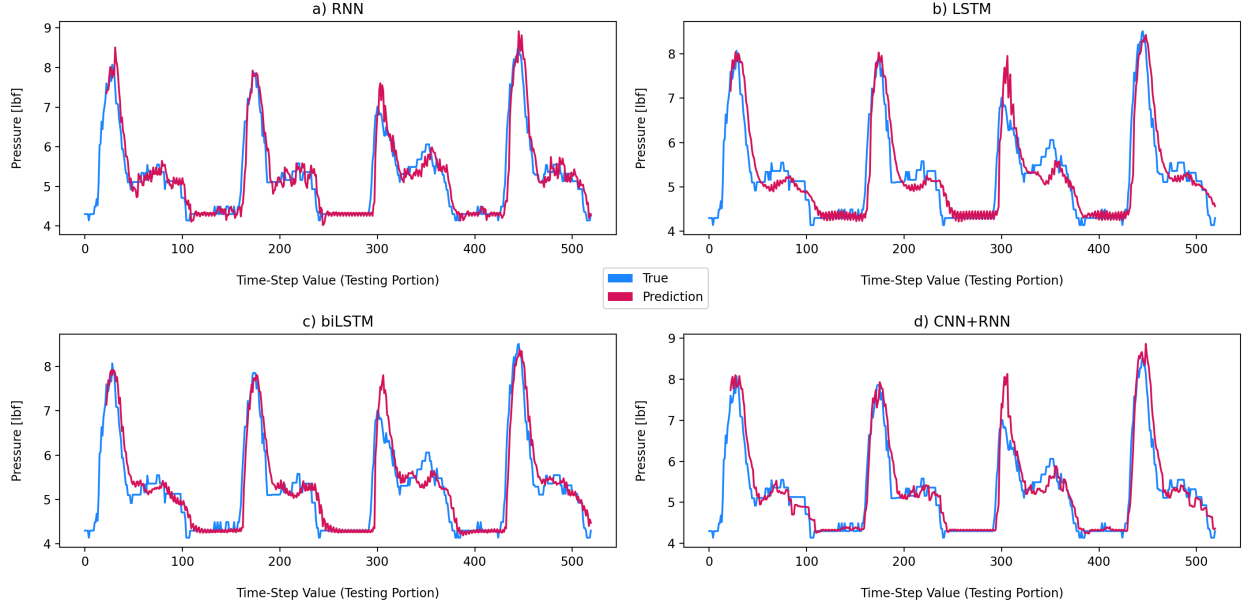


Figure 11: Setup by Participant: JM 20-3 Summed up Values for all (Sensors) True Test Data Values (blue) vs Predicted Data Values (red)

**Participant JM 20-5** Table 12 shows the numerical error values for participant JM for an input window value of 20 and output window value of 5 (referred to as JM 20-5). We present participants JM because they have the best RMSE value for CNN+RNN for a window size of 20-5 compared to other participants (for the same window size). Surprisingly, the biLSTM model slightly outperforms the CNN+RNN model (by about 0.005). The large input and large output window should allow the CNN+RNN model to perform the best, as it does for every other participant for this input and output window combination. With such a small difference in RMSE, it might still pay off to use CNN+RNN as it takes a shorter time to train, validate, and test than the biLSTM model (please see Table 2).

JG 20-5	MAE	MSE	RMSE
Simple	0.153473	0.073147	0.270456
LSTM	0.143723	0.065281	0.255501
biLSTM	0.130918	0.058085	0.241009
CNN RNN	0.091753	0.027673	0.166353

Table 13: Setup by Participant: JG 20-5 Error Metrics

**Participant JG 20-5** Table 13 shows the numerical error values for participant JG for an input window value of 20 and an output window value of 5 (referred to as JG 20-5). These results are the closest to the average values for all four models, as presented in Table 7. The CNN+RNN model outperforms all RNN models: simple RNN, LSTM, and biLSTM. CNN+RNN model excels due to the large input window size of 20 that provides additional history and context that helps the generation of accurate prediction for the large output size of 5. The large input size is an obstacle for RNN models that cannot keep up the accuracy for predicting as much as 5 consecutive output values.

*Discussion:* Our results indicate that the CNN+RNN models may be more capable and more suitable at *predicting long sequences of time-series data* than traditional advanced RNN methods. All of our experiments show that an increasing number of trials used for training (i.e. increased training length) in the ‘by participant’ setup does not correlate with the models having higher accuracy. We observe that the accuracy depends on the characteristics of the individual’s gait, which we leverage in our custom prediction models. Furthermore, all models for long-distance prediction are able to predict the entire trial in less than 0.11 sec, while CNN+RNN models took 0.088 sec, on average. Not only that the CNN+RNN models generate prediction in a shorter time, but also in the vast majority of cases they generate predictions with lower errors. We observed that in a few cases, CNN+RNN models slightly underperform compared to the biLSTM

models (for example in JM 20-5). With a very small difference in accuracy, the use of the CNN+RNN model may be a good tradeoff because it takes considerably less time to train and predict.

Additionally, as per our results, our models are able to *predict entire trial*. Our models are trained on varied numbers of concatenated trials, where one trial is used for validation, and one is used for testing. Consequently, the models make predictions for the *entire trial* with high accuracy for the setup ‘by participant’ designed for long-distance prediction (Table 7). This observation shows the applicability of the proposed value prediction to the target applications: for long-term or in-home monitoring and prognosis of recovery, fall prediction, or to aid the exoskeleton movement. For those applications, the training and validation would be done in a clinical setting (after the participant’s therapy or training sessions) when a desired goal has been achieved. Therefore, the models would capture Pareto-optimal gait patterns. The test data would be captured in an in-home setting. For recovery or fall prediction, the magnitude of the error between the predicted and captured data would indicate changes in the participant’s health or abilities. For aiding the exoskeleton movement, the predicted data values could be used to continue the sequence of exoskeleton movements after the participant initiates the movement in a certain direction. Additionally, the ‘by participant’ setup is suitable for authentication, where the training would be done for a set of known participants, and the errors between predicted and newly captured values would quantify the likelihood of the match to any of the known participants. The lack of match within a defined threshold can point to an unknown subject.

Our models are unique because they are customized and they predict values, rather than being trained for the entire participant population and classifying the participant’s trials into predefined classes. This is not only a contribution but also an indication of the applicability of our models for the above-mentioned applications.

## 6 Limitations and Future Directions

We propose future work to address the limitations of this study, but also to explore future software and hardware system design for a wider range of populations and applications.

Our study was performed using the data collected from healthy participants with an age range from 18 to 28, using data from the reference (right) foot. We will expand our work to include a wide range of ages and different health conditions while exploring the differences in gait (pressure) patterns for both legs. We will explore how the insight gained from value prediction can be used for diagnosis, in addition to progress assessment, rehabilitation, aiding exoskeleton movement, or authentication for individuals with different health conditions.

Our run-time data are estimates as they include the system overhead of the Google Cloud Platform. They are computed for each experiment: where for each trial/participant the training and validation are run once, and testing is run 1,000 times and the results are averaged. We recognize that the used hardware provides substantial computation, communication, and storage resources, hence we might not be able to achieve this speed on a more limited platform. Since the value prediction is targeted to be used in real-time applications, we need to extend the proposed approach to software system design where the cloud, edge, or micro-controller could host training or run the models to evaluate the performance. Due to considerations like data privacy, autonomy, and cost, Liberis et al. Liberis and Lane [2023] contain machine learning inference within the device itself. However, deep learning, especially training, with limited hardware resources is an extremely challenging problem. We plan to evaluate the trade-offs for communication, memory utilization, performance, battery life, and wearability for the future system.

Additionally, we will explore the application of different filters for raw data, such as a simple running average filter, which could improve training time, resource requirements, and testing run time. Burdack et al. Burdack et al. [2020] used filtering, time derivatives, and data scaling to preprocess the data obtained from Ground Reaction Force sensors. Such preprocessing was used for classification, but we may explore the use of some of those methods for value prediction. Additionally, deep learning itself could be used for feature extraction and data preprocessing Morbidoni et al. [2019], Costilla-Reyes et al. [2021].

While running our deep learning models, we did not employ N-fold cross-validation. We are questioning its application for real-time scenarios, as it implies random selection of a portion of a trial (for ‘by trial’ setup) or one of the trials (for ‘by participant’ setup). This kind of selection is not feasible for real-time applications as it needs prediction generated for the most recent trial, rather than a random trial. N-fold cross-validation is a possible approach for non-real-time applications, like authentication.

Our stretch goal is to develop an easy-to-use, inexpensive sensor-based system, accompanied by appropriate deep learning models to accurately assess movement disorders in gait, accurately predict fall risks, or aid exoskeleton movement for a wide range of individuals. We will research the use of several different sensor types, placed on various body parts to improve prediction accuracy or extend applicability to other movement or postural disorders. Finally, we plan to implement a conditional Generative Adversarial Network and Attention mechanism to further preserve

long-distance information loss. We also intend to make use of the pre-trained state-of-the-art deep neural network models to fine-tune our time series gait data.

## 7 Conclusions

We present a technique for the application of *customized* deep-learning models for a value prediction of gait spatiotemporal parameters, namely pressure sensor data. We compare and contrast short- and long-distance predictions in two different experimental setups, ‘by trial’ and ‘by participant’, respectively. As our models expand beyond classifiers, so do their applications. We target their use in a variety of health-related applications as well as for biometric authentication. The novelty of our work also extends to the application of deep learning models to time series of gait data, which despite the smaller number of features have high prediction accuracy.

Our results show that the best-performing model for a short sequence prediction is Bidirectional LSTM with an average RMSE = 0.124346 and a minimum RMSE = 0.060675. The best-performing model for long-distance prediction in the vast majority of cases is CNN+RNN with an average RMSE = 0.194171, and as low as RMSE = 0.106365. Moreover, the proposed CNN+RNN setup can accurately predict an entire trial, when trained and validated using the trials from the same participant. We illustrate prediction accuracy by plotting the sum of sensor values for each time step and the sum of predicted data for the corresponding time step.

Our future directions will be in the domains of exploring and possibly including a variety of sensors, fine-tuning the acquisition technique, expanding the approach to a wider population, and designing corresponding deep learning models to prove accuracy for extended application domains. Our goal is to explore hardware and software system design to achieve ease of use, accuracy, and affordability that will use gait data for health, well-being, and security applications.

## Acknowledgement

We would like to acknowledge Grayson Hill and Jessica Wei for their help with the engineering setup and discussion, and John Sanchez for his early work on surveying the related literature.

We would also like to thank all participants who volunteered for this study.

## References

- R. Baker, A. Esquenazi, Benedetti, M. G., and K. Desloovere. Gait analysis: clinical facts. *European Journal of Physical and Rehabilitation Medicine*, 52(4):560–574, 2016.
- Mobility lab by apdm wearable technologies. URL <https://apdm.com/mobility/>.
- Khoo I.-H., Marayong P., Krishnan V., Balagtas M. N., and Rojas O. Design of a biofeedback device for gait rehabilitation in post-stroke patients. In *Proc. IEEE 58th International Midwest Symposium on Circuits and Systems (MWSCAS)*, pages 1–4, 2015. doi:<https://doi.org/10.1109/mwscas.2015.7282097>.
- Joonbum Bae, Kyoungchul Kong, Nancy Byl, and Masayoshi Tomizuka. A mobile gait monitoring system for gait analysis. In *2009 IEEE International Conference on Rehabilitation Robotics*, pages 73–79, 2009. doi:10.1109/ICORR.2009.5209621.
- Kyoungchul Kong, Joonbum Bae, and Masayoshi Tomizuka. Detection of abnormalities in a human gait using smart shoes. *Proceedings of SPIE - The International Society for Optical Engineering*, 6932, 05 2008. doi:10.1117/12.776003.
- Andrea Mannini and Angelo Sabatini. A hidden markov model-based technique for gait segmentation using a foot-mounted gyroscope. In *In Proceedings of Annual International Conference of the IEEE Engineering in Medicine and Biology Society.*, pages 4369–73, 08 2011. doi:10.1109/IEMBS.2011.6091084.
- Sasanka Potluri, Arvind Beerjapalli Chandran, Christian Diedrich, and Lutz Schega. Machine learning based human gait segmentation with wearable sensor platform. In *2019 41st Annual International Conference of the IEEE Engineering in Medicine and Biology Society (EMBC)*, pages 588–594, 2019. doi:10.1109/EMBC.2019.8857509.
- Jucheol Moon, Nhat Anh Le, Nelson Hebert Minaya, and Sang-II Choi. Multimodal few-shot learning for gait recognition. *Applied Sciences*, 10(21), 2020a. ISSN 2076-3417. doi:10.3390/app10217619. URL <https://www.mdpi.com/2076-3417/10/21/7619>.
- Ruojun Li, Emmanuel Agu, Ganesh Balakrishnan, Debra Herman, Ana Abrantes, Michael Stein, and Jane Metrik. Weedgait: Unobtrusive smartphone sensing of marijuana-induced gait impairment by fusing gait cycle segmentation

- and neural networks. In *2019 IEEE Healthcare Innovations and Point of Care Technologies, (HI-POCT)*, pages 91–94, 2019. doi:10.1109/HI-POCT45284.2019.8962787.
- Nurul Fathiah Ghazali, Norazman Shahar, Nur Azmina Rahmad, Nur Anis Jasmin Sufri, Muhammad Amir As'ari, and H. F. M Latif. Common sport activity recognition using inertial sensor. *2018 IEEE 14th International Colloquium on Signal Processing & Its Applications (CSPA)*, pages 67–71, 2018.
- Sung-Sin Lee, Sang Tae Choi, and Sang-Il Choi. Classification of gait type based on deep learning using various sensors with smart insole. *Sensors*, 19(8), 2019a. ISSN 1424-8220. URL <https://www.mdpi.com/1424-8220/19/8/1757>.
- Min Hun Lee, Daniel P. Siewiorek, Asim Smailagic, Alexandre Bernardino, and Sergi Bermúdez i Badia. Learning to assess the quality of stroke rehabilitation exercises. In *Proceedings of the 24th International Conference on Intelligent User Interfaces, IUI '19*, page 218–228, New York, NY, USA, 2019b. Association for Computing Machinery. ISBN 9781450362726. doi:10.1145/3301275.3302273. URL <https://doi-org.csulb.idm.oclc.org/10.1145/3301275.3302273>.
- Erwin Aertbeliën and Joris De Schutter. Learning a predictive model of human gait for the control of a lower-limb exoskeleton. In *In Proceedings of 5th IEEE RAS/EMBS International Conference on Biomedical Robotics and Biomechatronics (BIROB 2014)*, 08 2014. doi:10.1109/BIROB.2014.6913830.
- Roman Schniepp, Anna Huppert, Julian Decker, Fabian Schenkel, Cornelia Schlick, Atal Rasoul, Marianne Dieterich, Thomas Brandt, Klaus Jahn, and Max Wühr. Fall prediction in neurological gait disorders: differential contributions from clinical assessment, gait analysis, and daily-life mobility monitoring. *Journal of Neurology*, 03 2021. doi:10.1007/s00415-021-10504-x.
- Kaiyu Tong and Malcolm H Granat. A practical gait analysis system using gyroscopes. *Medical Engineering and Physics*, 21(2):87–94, 1999. ISSN 1350-4533. doi:[https://doi.org/10.1016/S1350-4533\(99\)00030-2](https://doi.org/10.1016/S1350-4533(99)00030-2). URL <https://www.sciencedirect.com/science/article/pii/S1350453399000302>.
- A.M. Sabatini, C. Martelloni, S. Scapellato, and F. Cavallo. Assessment of walking features from foot inertial sensing. *IEEE Transactions on Biomedical Engineering*, 52(3):486–494, 2005. doi:10.1109/TBME.2004.840727.
- Jay Hertel Rachel M Koldenhoven. Validation of a wearable sensor for measuring running biomechanics. *Digit Biomark*, 2:74–78, 08 2018. doi:10.1159/000491645.
- Murai A., Shioyama C., Ming D., Takamatsu J., Tada M., and Ogasawara T. Estimation of running injury risks using wearable sensors. In *ISBS Proceedings Archive*, 36 (1), pages 240–243, February 2018. URL <https://commons.nmu.edu/isbs/vol36/iss1/30>.
- I-Hung Khoo, Panadda Marayong, Vennila Krishnan, Michael Balagtas, Omar Rojas, and Katherine Leyba. Real-time biofeedback device for gait rehabilitation of post-stroke patients. *Biomedical Engineering Letters*, 7, 06 2017. doi:10.1007/s13534-017-0036-1.
- Joonbum Bae and Masayoshi Tomizuka. Gait phase analysis based on a hidden markov model. *Mechatronics*, 21(6):961–970, 2011. ISSN 0957-4158. doi:<https://doi.org/10.1016/j.mechatronics.2011.03.003>. URL <https://www.sciencedirect.com/science/article/pii/S0957415811000481>.
- Omar Costilla-Reyes, Ruben Vera-Rodriguez, Abdullah S. Alharthi, Syed U. Yunus, and Krikor B. Ozanyan. *Deep Learning in Gait Analysis for Security and Healthcare*, pages 299–334. Springer International Publishing, Cham, 2020. ISBN 978-3-030-31760-7. doi:10.1007/978-3-030-31760-7\_10. URL [https://doi.org/10.1007/978-3-030-31760-7\\_10](https://doi.org/10.1007/978-3-030-31760-7_10).
- Jindong Wang, Yiqiang Chen, Shuji Hao, Xiaohui Peng, and Lisha Hu. Deep learning for sensor-based activity recognition: A survey. *Pattern Recognition Letters*, 119:3–11, 2019. ISSN 0167-8655. doi:<https://doi.org/10.1016/j.patrec.2018.02.010>. URL <https://www.sciencedirect.com/science/article/pii/S016786551830045X>. Deep Learning for Pattern Recognition.
- J. Parkka, M. Ermes, P. Korpiainen, J. Mantyjarvi, J. Peltola, and I. Korhonen. Activity classification using realistic data from wearable sensors. *IEEE Transactions on Information Technology in Biomedicine*, 10(1):119–128, 2006. doi:10.1109/TITB.2005.856863.
- Footlogger. URL <http://www.footlogger.com/>.
- Jucheol Moon, Nelson Hebert Minaya, Nhat Anh Le, Hee-Chan Park, and Sang-Il Choi. Can ensemble deep learning identify people by their gait using data collected from multi-modal sensors in their insole? *Sensors*, 20(14), 2020b. ISSN 1424-8220. doi:10.3390/s20144001. URL <https://www.mdpi.com/1424-8220/20/14/4001>.
- Huanghe Zhang, Yi Guo, and Damiano Zanon. Accurate ambulatory gait analysis in walking and running using machine learning models. *IEEE Transactions on Neural Systems and Rehabilitation Engineering*, 28(1):191–202, 2020. doi:10.1109/TNSRE.2019.2958679.

- Yi Xia, Jun Zhang, Qiang Ye, Nan Cheng, Yixiang Lu, and Dexiang Zhang. Evaluation of deep convolutional neural networks for detection of freezing of gait in parkinson's disease patients. *Biomedical Signal Processing and Control*, 46:221–230, 2018.
- Yuqing Chen and Yang Xue. A deep learning approach to human activity recognition based on single accelerometer. *2015 IEEE International Conference on Systems, Man, and Cybernetics*, pages 1488–1492, 2015.
- Fabian Horst, S. Lapuschkin, W. Samek, K. Müller, and W. Schöllhorn. Explaining the unique nature of individual gait patterns with deep learning. *Scientific Reports*, 9, 2019.
- Samir A. Rawashdeh, Derek A. Rafeldt, and Timothy L. Uhl. Wearable imu for shoulder injury prevention in overhead sports. *Sensors*, 16(11), 2016. ISSN 1424-8220. doi:10.3390/s16111847. URL <https://www.mdpi.com/1424-8220/16/11/1847>.
- Andrey Rudenko, Luigi Palmieri, Michael Herman, Kris M Kitani, Dariu M Gavrilă, and Kai O Arras. Human motion trajectory prediction: A survey. *Int. J. Rob. Res.*, 39(8):895–935, jul 2020. ISSN 0278-3649. doi:10.1177/0278364920917446. URL <https://doi.org/10.1177/0278364920917446>.
- Khaled Saleh, Mohammed Hossny, and Saeid Nahavandi. Intent prediction of pedestrians via motion trajectories using stacked recurrent neural networks. *IEEE Transactions on Intelligent Vehicles*, 3(4):414–424, 2018. doi:10.1109/TIV.2018.2873901.
- Nemanja Djuric, Vladan Radosavljevic, Henggang Cui, Thi Nguyen, Fang-Chieh Chou, Tsung-Han Lin, and Jeff Schneider. Motion prediction of traffic actors for autonomous driving using deep convolutional networks. *CoRR*, abs/1808.05819, 2018. URL <http://arxiv.org/abs/1808.05819>.
- Hao Xue, Du Q. Huynh, and Mark Reynolds. Ss-lstm: A hierarchical lstm model for pedestrian trajectory prediction. In *2018 IEEE Winter Conference on Applications of Computer Vision (WACV)*, pages 1186–1194, 2018. doi:10.1109/WACV.2018.00135.
- Tianyang Zhao, Yifei Xu, Mathew Monfort, Wongun Choi, Chris Baker, Yibiao Zhao, Yizhou Wang, and Ying Nian Wu. Multi-agent tensor fusion for contextual trajectory prediction. In *Proceedings of the IEEE/CVF Conference on Computer Vision and Pattern Recognition*, pages 12126–12134, 2019.
- Kunihiro Ogata and Yoshio Matsumoto. Estimating movements of human body for the shirt-type wearable device mounted on the strain sensors based on convolutional neural networks. In *2019 41st Annual International Conference of the IEEE Engineering in Medicine and Biology Society (EMBC)*, pages 5871–5876, 2019. doi:10.1109/EMBC.2019.8856722.
- Elsa J. Harris, I-Hung Khoo, and Emel Demircan. A survey of human gait-based artificial intelligence applications. *Frontiers in Robotics and AI*, 8, 2022. ISSN 2296-9144. doi:10.3389/frobt.2021.749274. URL <https://www.frontiersin.org/articles/10.3389/frobt.2021.749274>.
- Abdul Saboor, Triin Kask, Alar Kuusik, Muhammad Mahtab Alam, Yannick Le Moullec, Imran Khan Niazi, Ahmed Zoha, and Rizwan Ahmad. Latest research trends in gait analysis using wearable sensors and machine learning: A systematic review. *IEEE Access*, 8:167830–167864, 2020.
- Lingmei Ren and Yanjun Peng. Research of fall detection and fall prevention technologies: A systematic review. *IEEE Access*, 7:77702–77722, 2019. doi:10.1109/ACCESS.2019.2922708.
- J. Lasselín, T. Sundelin, P.M. Wayne, M.J. Olsson, S. Paues Göranson, J. Axelsson, and M. Lekander. Biological motion during inflammation in humans. *Brain, Behavior, and Immunity*, 84:147–153, 2020. ISSN 0889-1591. doi:<https://doi.org/10.1016/j.bbi.2019.11.019>. URL <https://www.sciencedirect.com/science/article/pii/S0889159119306427>.
- Damla Arifoglu and Abdelhamid Bouchachia. Activity recognition and abnormal behaviour detection with recurrent neural networks. *Procedia Computer Science*, 110:86–93, 2017. ISSN 1877-0509. doi:<https://doi.org/10.1016/j.procs.2017.06.121>. URL <https://www.sciencedirect.com/science/article/pii/S1877050917313005>. 14th International Conference on Mobile Systems and Pervasive Computing (MobiSPC 2017) / 12th International Conference on Future Networks and Communications (FNC 2017) / Affiliated Workshops.
- Brian Russell, Andrew McDaid, William Toscano, and Patria Hume. Moving the lab into the mountains: A pilot study of human activity recognition in unstructured environments. *Sensors*, 21(2), 2021. ISSN 1424-8220. doi:10.3390/s21020654. URL <https://www.mdpi.com/1424-8220/21/2/654>.
- Wei-Yi Cheng, Alf Scotland, Florian Lipsmeier, Timothy Kilchenmann, Liping Jin, Jens Schjodt-Eriksen, Detlef Wolf, Yan-Ping Zhang Schäfer, Ignacio Fernandez Garcia, Juliane Siebourg-Polster, Jay Soto, Lynne Verselis, Meret Martin-Facklam, Frank Boess, Martin Koller, Michael Grundman, Andreas U. Monsch, Ronald B. Postuma, Anirvan Ghosh, Thomas Kremer, Kirsten I. Taylor, Christian Czech, Christian Gossens, and Michael Lindemann. Human activity recognition from sensor-based large-scale continuous monitoring of parkinson's disease patients. *2017*

- IEEE/ACM International Conference on Connected Health: Applications, Systems and Engineering Technologies (CHASE)*, pages 249–250, 2017.
- Ryan S. McGinnis, Nikhil Mahadevan, Yaejin Moon, Kirsten Seagers, Nirav Sheth, Jr. John A. Wright, Steven DiCristofaro, Ikaro Silva, Elise Jortberg, Melissa Ceruolo, Jesus A. Pindado, Jacob Sosnoff, Roozbeh Ghaffari, and Shyamal Patel. A machine learning approach for gait speed estimation using skin-mounted wearable sensors: From healthy controls to individuals with multiple sclerosis. *PLoS One*, 2017. doi:doi:10.1371/journal.pone.0178366.
- Yongjia Zhao and Suiping Zhou. Wearable device-based gait recognition using angle embedded gait dynamic images and a convolutional neural network. *Sensors*, 17(3), 2017. ISSN 1424-8220. doi:10.3390/s17030478. URL <https://www.mdpi.com/1424-8220/17/3/478>.
- Christian Janiesch, Patrick Zschech, and Kai Heinrich. Machine learning and deep learning. *Electron Markets*, 31: 685–695, 2021. doi:<https://doi.org/10.1007/s12525-021-00475-2>.
- Yann LeCun, Léon Bottou, Yoshua Bengio, and Patrick Haffner. Gradient-based learning applied to document recognition. *Proceedings of the IEEE*, 86(11):2278–2324, 1998.
- Alex Krizhevsky, Ilya Sutskever, and Geoffrey E Hinton. Imagenet classification with deep convolutional neural networks. In *Advances in neural information processing systems*, pages 1097–1105, 2012.
- Christian Szegedy, Wei Liu, Yangqing Jia, Pierre Sermanet, Scott Reed, Dragomir Anguelov, Dumitru Erhan, Vincent Vanhoucke, and Andrew Rabinovich. Going deeper with convolutions. In *Proceedings of the IEEE conference on computer vision and pattern recognition*, pages 1–9, 2015.
- Karen Simonyan and Andrew Zisserman. Very deep convolutional networks for large-scale image recognition. *arXiv preprint arXiv:1409.1556*, 2014.
- John F Kolen and Stefan C Kremer. *A field guide to dynamical recurrent networks*. John Wiley & Sons, 2001.
- Razvan Pascanu, Tomas Mikolov, and Yoshua Bengio. On the difficulty of training recurrent neural networks. In *International conference on machine learning*, pages 1310–1318, 2013.
- Razvan Pascanu, Tomas Mikolov, and Yoshua Bengio. Understanding the exploding gradient problem. *CoRR*, *abs/1211.5063*, 2:417, 2012.
- Andrej Karpathy, Justin Johnson, and Li Fei-Fei. Visualizing and understanding recurrent networks. *arXiv preprint arXiv:1506.02078*, 2015.
- Jianjun Ni, Yinan Chen, Yan Chen, Jinxiu Zhu, Deena Ali, and Weidong Cao. A survey on theories and applications for self-driving cars based on deep learning methods. *Applied Sciences*, 10(8), 2020. ISSN 2076-3417. doi:10.3390/app10082749. URL <https://www.mdpi.com/2076-3417/10/8/2749>.
- Shaoqing Ren, Kaiming He, Ross Girshick, and Jian Sun. Faster r-cnn: Towards real-time object detection with region proposal networks. *arXiv preprint arXiv:1506.01497*, 2015.
- Kaiming He, Georgia Gkioxari, Piotr Dollár, and Ross Girshick. Mask r-cnn. In *Proceedings of the IEEE international conference on computer vision*, pages 2961–2969, 2017.
- Ashish Vaswani, Noam Shazeer, Niki Parmar, Jakob Uszkoreit, Llion Jones, Aidan N Gomez, Lukasz Kaiser, and Illia Polosukhin. Attention is all you need. *arXiv preprint arXiv:1706.03762*, 2017.
- Wenlu Zhang, Lusi Li, Vincent Cheong, Bo Fu, and Mehrdad Aliasgari. Deep encoder–decoder neural networks for retinal blood vessels dense prediction. *International Journal of Computational Intelligence Systems*, 14(1): 1078–1086, 2021.
- Wenlu Zhang, Rongjian Li, Houtao Deng, Li Wang, Weili Lin, Shuiwang Ji, and Dinggang Shen. Deep convolutional neural networks for multi-modality iso-intense infant brain image segmentation. *NeuroImage*, 108:214–224, 2015.
- Sunitha Basodi, Chunyan Ji, Haiping Zhang, and Yi Pan. Gradient amplification: An efficient way to train deep neural networks. *Big Data Mining and Analytics*, 3(3):196–207, 2020. doi:10.26599/BDMA.2020.9020004.
- Sepp Hochreiter and Jürgen Schmidhuber. Long short-term memory. *Neural computation*, 9(8):1735–1780, 1997.
- Mike Schuster and Kuldip K Paliwal. Bidirectional recurrent neural networks. *IEEE Transactions on Signal Processing*, 45(11):2673–2681, 1997.
- Kaiming He, Xiangyu Zhang, Shaoqing Ren, and Jian Sun. Deep residual learning for image recognition. In *Proceedings of the IEEE conference on computer vision and pattern recognition*, pages 770–778, 2016.
- Yang Liu, Jelena Trajkovic, Hen-Geul Henry Yeh, and Wenlu Zhang. Machine learning for predicting stock market movement using news headlines. In *2020 IEEE Green Energy and Smart Systems Conference (IGESSC)*, pages 1–6, 2020. doi:10.1109/IGESSC50231.2020.9285163.

- Avraam Tsantekidis, Nikolaos Passalis, Anastasios Tefas, Juho Kannianen, Moncef Gabbouj, and Alexandros Iosifidis. Forecasting stock prices from the limit order book using convolutional neural networks. In *2017 IEEE 19th Conference on Business Informatics (CBI)*, volume 01, pages 7–12, 2017. doi:10.1109/CBI.2017.23.
- Tian Shi, Yaser Keneshloo, Naren Ramakrishnan, and Chandan K Reddy. Neural abstractive text summarization with sequence-to-sequence models. *ACM Transactions on Data Science*, 2(1):1–37, 2021.
- Adam optimizer keras. URL <https://keras.io/api/optimizers/adam/>.
- Rmsprop optimizer keras. URL <https://keras.io/api/optimizers/rmsprop/>.
- Edgar Liberis and Nicholas D. Lane. Differentiable neural network pruning to enable smart applications on microcontrollers. 6(4), jan 2023. doi:10.1145/3569468. URL <https://doi.org/10.1145/3569468>.
- J. Burdack, F. Horst, S. Giesselbach, I. Hassan, S. Daffner, and W. I. Schöllhorn. Age-related differences in healthy adults walking patterns under a cognitive task with deep neural networks. *Frontiers in Bioengineering and Biotechnology*, 8:260, 2020. doi:<https://doi.org/10.3389/fbioe.2020.00260>.
- Christian Morbidoni, Alessandro Cucchiarelli, Sandro Fioretti, and Francesco Di Nardo. A deep learning approach to emg-based classification of gait phases during level ground walking. *Electronics*, 8(8):894, Aug 2019. ISSN 2079-9292. doi:10.3390/electronics8080894. URL <http://dx.doi.org/10.3390/electronics8080894>.
- Omar Costilla-Reyes, Patricia Scully, Iracema Leroi, and Krikor B. Ozanyan. Age-related differences in healthy adults walking patterns under a cognitive task with deep neural networks. *IEEE Sensors Journal*, 21(2):2353–2363, 2021. doi:10.1109/JSEN.2020.3021349.